Spin-Orbit Alignment: Interactions between a Pre-Main Sequence Star and a Binary Black Hole

By

Hans D. Vanderzyden

Department of Physics

Allegheny College

Meadville, Pennsylvania

April, 2025

Spin-Orbit Alignment: Interactions between a Pre-Main Sequence Star and a Binary Black Hole

By

Hans D. Vanderzyden

Department of Physics

Allegheny College

Meadville, Pennsylvania

April, 2025

Submitted in fulfillment of the senior thesis requirements of the
Department of Physics at Allegheny College
and approved by the senior thesis committee.

Dr. James C. Lombardi, Jr.	**Date**	***Dr. Adelé Poynor***	**Date**

Pledge

Table of Contents

Acknowledgements 7

Abstract 9

1. Introduction and Background 10

1.1 Motivation 10

1.2 Prior Work 10

2. Theory 12

2.1 Gravity 12

2.1.1 Laws of Motion 12

2.1.2 Newton's Law of Universal Gravitation 13

2.2 Stars 14

2.2.1 Density, Hydrostatic Equilibrium, and Pressure 14

2.2.2 Evolutionary Stages 16

2.2.3 Globular Clusters 19

2.3 Black Holes 20

2.3.1 Schwarzschild Radius 20

2.3.2 Tidal Force and Tidal Radius 22

2.3.3 Tidal Disruption Events 23

2.3.4 Binary Black Holes 24

2.3.5 Interaction Timescales 27

2.4 Gravitational Waves 29

2.4.1 Laser Interferometers for Observing Gravitational Waves 29

2.4.2 The Dimensionless Spin Parameter, χeff 31

2.5 Rotations and Orbits 33

2.5.1 The Six Degrees of Freedom of Orbits 34

2.5.2 Circular, Elliptical, Parabolic, and Hyperbolic Orbits 35

2.5.3 Conservation of Angular Momentum 36

2.5.4 Orbital Dynamics 36

2.5.5 Gravity Assist 38

2.5.6 Kick Velocity 40

3. Methodology 41
3.1 Cluster Monte Carlo Code 42
3.2 Modules for Experiments in Stellar Astrophysics Code 43
3.3 Pre-Collision Trajectory Three-Body Integrator Code 44
3.4 *StarSmasher* Code 45
3.4.1 Smoothed-Particle Hydrodynamics 46
3.4.2 Relaxations 47
3.4.3 Dynamical Collisions 50
3.5 Post-Processing Analysis 50
4. Results and Analysis 51
4.1 Collision Probabilities 56
4.2 Positive χ_{eff} Convergence 58
4.3 χ_{eff} Flip Criteria and Outcomes for Coplanar Cases 59
4.4 Dynamical Outcomes 62
5. Conclusion 67
5.1 Future Work 68
Bibliography 70
Appendix A 73

List of Figures

Figure 1: An inferred χeff cumulative distribution function for the BBH population in Fishbach et al (2022).....11
Figure 2: Hydrostatic Equilibrium in a pre-MS star. 16
Figure 3: An HR diagram showing all the different possible evolutionary tracks for a star [7]. .17
Figure 4: The three possible stages of the pp chain. 18
Figure 5: The components of a BH. 21
Figure 6: The tidal radius, rt. 23
Figure 7: BBH formation through dynamical assembly. 25
Figure 8: BBH formation through isolated binary evolution. 26
Figure 9: BBH formation through chemically homogenous evolution. 27
Figure 10: A basic blueprint of the Michelson Interferometer used at LIGO and other observatories [15]. 31
Figure 11: The three different extreme relationships between $LBBH$ and $Ldisk$ to set boundary conditions on χeff values (from -1 to 1). 33
Figure 12: The semi-major (a) and semi-minor (b) axes, apoapsis and periapsis, and true anomaly (ν) [16]. 34
Figure 13: The argument of periapsis (ω), inclination (i), longitude of the ascending node (Ω), and true anomaly (ν). 34
Figure 14: How gravity assist increases the velocity of a spacecraft passing behind a planet's direction of inertial motion [17]. 39
Figure 15: Gravity assist visualized by special relativity. 40
Figure 16: The methodology of this research. 42
Figure 17: Northwestern CMC data with Allegheny SPH scenarios overlaid [3]. 43
Figure 18: An H-R diagram for scenario #2 and #3's MESA model stars later used for SPH calculations in StarSmasher. 44
Figure 19: An example of three-body integration of a collision case for scenario #2. 45
Figure 20: Visual representation of an SPH Wendland C4 kernel. 46
Figure 21: 9.6 $M\odot$ MS star (scenario #2) relaxation, visualized using SPLASH [28]. 47
Figure 22: Energy vs. time plots for scenario #2's star SPH relaxation. 48
Figure 23: Various values vs. radius of the relaxing scenario #2 star. 49
Figure 24: Visualization of Case #21 in SPLASH as a column density, which is 3-dimensional density projected onto the 2-dimensional x-y plane [28]. 54
Figure 25: Case #21's mass ejection from SPH due to a fast-forming tight binary. 55
Figure 26: Various angular momenta and spins plotted together along with the total angular momentum of the system vs. time in code units. 56
Figure 27: Probability plot for scenario #2. 58
Figure 28: χeff vs. $time$ for all scenario #2 StarSmasher simulations. 59

Figure 29: Case #1: An example of no spin flip with velocity vectors overlaid and BH1 visually centered. 60
Figure 30: Case #2: An example of spin flip with velocity vectors overlaid and BH1 visually centered. 61
Figure 31: Various spins and masses vs. time for cases #1 (no spin flip) and #2 (spin flip).....61
Figure 32: Inspiral time vs. kick velocity for all cases. 63
Figure 33: Final BBH eccentricity vs. the composite variable $A = L\mathrm{BBH,f}2a\mathrm{BBH,f}$, with SPH data represented as blue dots and equation 2.5.10 as the solid and dashed lines, and $t\mathrm{GW}$ values written next to each case. 64
Figure 34: Total BBH energy vs. total BBH angular momentum for all 21 dynamical simulations.....65
Figure 35: Relationship between the inspiral time ratio and change in BBH angular momentum. 66
Figure 36: Relationship between the inspiral ratio and initial total system angular momentum. 67

List of Tables

Table 1: Initial values for the chosen CMC scenarios (before collision). 43
Table 2: All 22 simulations for scenario #2: the 9.6 $M\odot$ pre-MS star interacting with the 57.0 $M\odot$ BBH. 52
Table 3: A continuation of Table 2, but with physical data. 53

Acknowledgements

First, I would like to thank my advisor, Dr. Lombardi. Ever since my first semester here you have been a fantastic mentor for everything academically and have always been free to talk, which I greatly appreciate. I treasure you welcoming me into your research lab in just my second semester on campus as this has propelled me to the many of research experiences I have had from Allegheny and beyond. Thank you for going out of your way to allow me to participate in URSCA during the summer of 2023 and always being willing to write me a letter of recommendation. You have always pushed me to be the best student I can, both at Allegheny and beyond, and for that I am very grateful.

To my second reader, Dr. Petasis, thank you for the outside-of-astrophysics point of view towards physics and teaching me superior studying methods with the introductory to quantum mechanics course. Learning about your deviation from astrophysics in your undergraduate education has provided me with more hope about switching my field of study from astrophysics to nuclear engineering, and I appreciate that.

To the SPH research group at Northwestern, thank you for all the input and opportunities you have provided me. Thank you specifically to Fulya Kıroğlu for assisting me with your professional level of experience in this subject and for allowing me to work with you on past projects. Our work has closely aligned with both my URSCA and Comp projects, and I am very grateful for your time and help.

To the fellow Stellar Bagel Lab students, thank you for creating a healthy research environment that makes my time there fun and exciting. I would like to specifically thank Charlie Gibson for always being there since we first joined the lab in our second semester at Allegheny. From the numerous classes we have had together to the independent study projects we have worked on together, I appreciate all your hard work!

To my family, thank you for always being there if I want to chat and supporting me in my academic endeavors. Although you may not know much about physics, the responsibility and work ethic that you grew me up on has propelled me to chase these goals. I will always appreciate your stable help that has allowed me to focus on my education to achieve my goals. I love you!

To NealeyClare, thank you for always being there for me. Thank you for listening to me rant about my research and schoolwork. Your energy always lightens my mood, especially after a long day in the lab or working on assignments. Thank you for picking me up when I'm down and pushing me to my limits. I love you!

To the Brothers of Phi Delta Theta, thank you for always being there to chat or hang out to alleviate any stress. I appreciate you all pushing me to not only excel in my leadership positions as a Brother, but also academically. I will always be grateful for this Chapter and the experiences I have had with it.

Spin-Orbit Alignment: Interactions between a Pre-Main Sequence Star and a Binary Black Hole

Hans D. Vanderzyden

Abstract

Main sequence stars are the most common type of star in the universe. Pre-main sequence stars are the precursors to main sequence stars, making their evolution crucial to study. Binary black holes are far less common, but the gravitational wave signals produced by them allow us to learn about these mysterious bodies. When stars interact with black holes, stellar mass can be stripped onto the black hole in an accretion disk, which alters the mass and spin of the black hole. These changes alter the magnitude of the gravitational wave signals detected from Earth. The most abundant collection of stars is globular clusters, where tens to hundreds of thousands of stars are housed. This project aims to analyze many different orbital geometries of a $9.6\ M_\odot$ main sequence star interacting with a $57\ M_\odot$ binary black hole by studying its effects on spin using the dimensionless spin parameter χ_{eff} and alterations in the binary black hole merger time after an interaction. Laser Interferometer Gravitational Wave Observatory data suggests that such dynamical interactions will produce a χ_{eff} distribution centered around small but positive values rather than a possibly expected random distribution centered around $\chi_{\text{eff}} = 0$. This study, with the help of the smoothed-particle hydrodynamics code *StarSmasher*, provides evidence to support this claim, with all cases ending with positive χ_{eff}.

1. Introduction and Background

1.1 Motivation

The mysterious interactions between binary black holes (BBHs) and stars motivate this research. My goal is to research simulations of collisions between pre-main sequence (pre-MS) stars and BBHs to find which cases most commonly lead to a positive correlation between the angular momentum of the BBH and the spin of the black holes (BHs) after collision. Some parameters that I will focus on include the orbital configurations, the masses of the objects, and angular momenta differences between the star and BBH before the collision. I hope to find a correlation between these factors and positive angular momentum-spin alignment.

This alignment is measured using the dimensionless spin parameter χ_{eff}, which can be calculated from simulations as well as empirical data from laser interferometers such as the Laser Interferometer Gravitational-Wave Observatory (LIGO). This parameter allows us to understand the effects of different characteristics of a star-BBH system on the BHs and their spins. The motivation behind using MS stars is commonality in stellar clusters, where lots of collisions between celestial bodies occur.

1.2 Prior Work

There have been many prior studies on interactions between stars and BHs. For example, Lopez et al [1] studies collisions between stars and BBHs in dense stellar clusters. They explain that BBHs in stellar clusters will lead to lots of interactions with stars, and these interactions can cause lots of stellar debris to be accreted onto the BHs, ultimately altering the spins of the BHs (and therefore their χ_{eff} values) [1]. A conclusion made in the paper is that mass accretion is an important factor in altering the spins of the BHs. They also state that although dynamically formed BBHs are expected to have random spin orientations, the spins can be altered by collisions. Studying dynamically formed BBHs, I hope to prove spin changes post-collision with simulations of these events.

Another study focusing on χ_{eff} is Fishbach et al. [2], which focuses on the most negative χ_{eff} systems formed from hierarchical BH mergers (HMs): BHs formed from multiple previous

mergers of other less massive BHs. They hope to prove what percentage of BBH formations are from HMs. The dimensionless spin parameter χ_{eff}, discussed further in Section 2.4.2, is the mass-weighted total spin of the system in the direction of the orbital angular momentum of the BBH. The formation channel of a BBH can be distinguished by statistics of the χ_{eff} values, with dynamical assembly leading to random spin orientations, but isolated binary evolution leads to preferential spin alignment, discussed further in Section 2.3.4 [2]. χ_{eff} values, ranging from -1 to +1, have been empirically calculated to be slightly positive on average, and Fishbach et al. shows this trend for empirical data from a LIGO-Virgo-KAGRA (LVK) catalog, GWTC-3, as shown in Figure 1 [2].

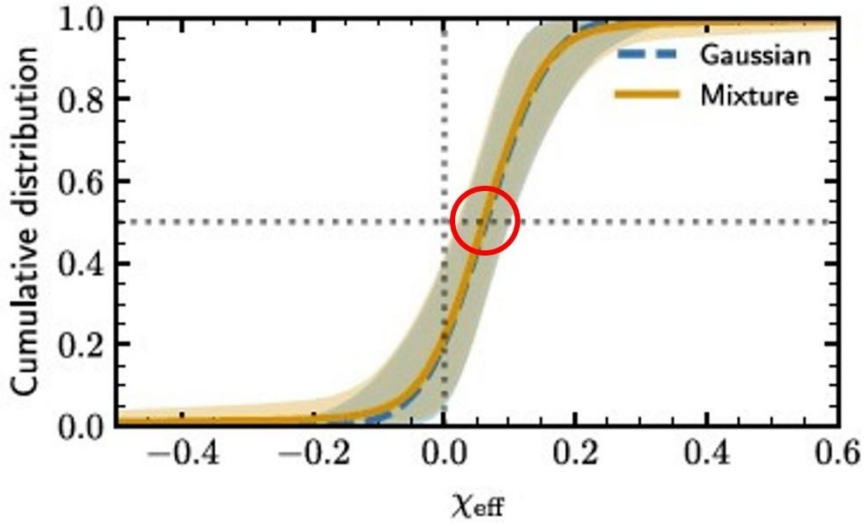


Figure 1: An inferred χ_{eff} cumulative distribution function for the BBH population in Fishbach et al (2022). This graph fits data from an LVK catalog, GWTC-3. They use both a gaussian fit (blue) and a mixture model between a gaussian and uniform distribution (orange). The shaded region shows the 90% credible interval. The plots show an average slight positive distribution in χ_{eff} values (with the red circle showing where the distribution is centered), and the low χ_{eff} limit helps motivate the fraction of systems that include HM products.

LVK catalog data shows no observations with $\chi_{\text{eff}} \lesssim -0.2$ [2]. Supporting this, Fishbach et al.'s data concludes that fewer than 4.2% of BBH systems in the astrophysical population have $\chi_{\text{eff}} < -0.3$, which provides an upper limit on the fraction of HM products in the population [2]. From χ_{eff} values inferred from LVK data; Fishbach et al. found that 26% of the systems in the underlying BBH population include HM products [2]. Although HMs are not the formation channel I am studying, these results help reinforce the slight positive χ_{eff} trends seen from the empirical LVK data.

A third study that motivates this work is Kıroğlu et al. [3], which studies spin-orbit

alignment of BBHs through accretion in young star clusters. Motivation for this research is that merging BBHs in young star clusters can undergo an accretion phase through stellar collisions, which can alter the BH spin vectors to align with the BBH orbital angular momentum [3]. This study conducts hydrodynamic simulations of MS stars colliding with BBHs to identify conditions that lead to spin-orbit alignment, like what I am studying [3]. One preliminary finding is that the outcomes rely heavily on the star-BBH mass ratio, $M_*/M_{\rm BBH}$, and the ratio of the orbital semi-major axis to the stellar radius, $a_{\rm BBH}/R_*$. These factors are plotted for *Cluster Monte Carlo (CMC)* data to show the most prominent star-BBH scenarios, which is discussed more in Section 3.1 and Figure 17. I have worked closely with the first author, Fulya Kıroğlu, on similar research, which motivates this project [4].

2. Theory

2.1 Gravity

The most prevalent yet invisible phenomenon in nature is gravity. Gravity is a fundamental interaction that causes an attraction between all objects that have mass. Gravity is responsible for orbits, the creation and evolution of stars and black holes, and much more.

2.1.1 Laws of Motion

Isaac Newton's three laws of motion describe the motion of any particle or object with mass. Newton's First Law, also known as the Law of Inertia, states that an object at rest or constant velocity will stay in these states unless acted on by an outside force. This helps describe why objects in a vacuum, such as space, will continue to move unless acted on by some gravitational force [5].

The most popular equation that is taught in the most introductory physics course is Newton's second law of motion, described by,

$$\vec{F} = \frac{d\vec{p}}{dt} = m\vec{a}, \tag{2.1.1}$$

where $\vec{F}$ is the net force vector acting on the object or system, $d\vec{p}$ is the momentum differential vector of the object or system, dt is the time differential, m is the mass of the object or system, and $\vec{a}$ is the acceleration vector of the object or system [5]. Since m can be used as the center of mass, Equation 2.1.1 is often used to calculate individual interactions between many particles in a system, which is later shown to be the backbone of the code *StarSmasher*.

The next important law of motion is Newton's third law,

$$\vec{F}_{12} = -\vec{F}_{21} \tag{2.1.2}$$

where $\vec{F}_{12}$ is the force vector of object 1 on object 2 and $\vec{F}_{21}$ is the force vector of object 2 on object 1 [5]. This law states that every force has an equal and opposite reactive force. This allows for an interaction between particles of distinct masses to cause different final accelerations, as shown by Equation 2.1.1. Equation 2.1.2 is implemented the same way as Equation 2.1.1, with each individual particle-particle interaction exerting an equal and opposite force on one another, causing changes in the kinematics, or movement, for members of the system.

2.1.2 Newton's Law of Universal Gravitation

A vital aspect of astrophysical calculations involves Newton's law of gravitation. This law focuses on gravitational interactions between celestial objects. Our smoothed-particle hydrodynamics (SPH) code *StarSmasher* calculates forces on each particle-particle interaction for every time step using Equation 2.1.3 [6]. With object 1 exerting a force on object 2, this law is expressed as

$$\vec{F}_{12} = -G\frac{m_1 m_2}{|\vec{r}_{12}|^2}\hat{r}_{12} \tag{2.1.3}$$

where G is the universal gravitational constant with a value of $6.673 * 10^{-11}$ $\mathrm{Nm^2kg^{-2}}$, m_1 and m_2 are the masses of objects 1 and 2, $|\vec{r}_{12}|$ is the distance between object 1 and object 2, and $\hat{r}$ is the unit vector representing the direction of the force from object 1 to object 2 [5]. This can also be represented for the force of object 2 on object 1 with the use of $\hat{r}_{21}$. The negative sign indicates that this is an attractive force.

2.2 Stars

The most abundant celestial objects in the universe are stars, with 100 billion stars in our own Milky Way galaxy! Stars are fantastic in that they emit powerful visible and invisible electromagnetic radiation, allowing us to view and detect them from Earth. Our favorite star is the Sun, which allowed the birth of Earth and provides us with consistent warmth and light. Due to its proximity to us, its physical and chemical properties have been studied quite well, and we often compare the characteristics of other stars to the Sun's. Throughout the rest of the paper, any quantities with a subscript ⊙ represent that of the Sun, and those with a subscript * represent that of a general star.

2.2.1 Density, Hydrostatic Equilibrium, and Pressure

When modeling a star, the three important physical characteristics to keep track of are density, hydrostatic equilibrium, and pressure.

Density is generally represented as a mass/volume. Assuming a spherical star, the average density is represented as

$$\rho = \frac{M_*}{\frac{4}{3}\pi R_*^3} \tag{2.2.1}$$

where M_* and R_* are the mass and radius of the star, respectively.

As discussed in Section 2.1.2, the gravitational force is always attractive. Because of this, inside a star, there must be another force counteracting it to avoid collapse. This is provided by pressure due to the hydrostatic equilibrium condition,

$$\frac{dP}{dr} = -G\frac{M_r\rho}{r^2} = -\rho g \tag{2.2.2}$$

where M_r is the enclosed mass inside a sphere of radius r, and $g = G\frac{M_r}{r^2}$ is the local gravitational acceleration at a radius r [5]. This condition assumes that the star is static, meaning the acceleration is zero. In *StarSmasher*, relaxation (as explained in Section 3.4.2) aims to reach hydrostatic equilibrium.

Pressure is generally represented as a force/area. In a star, there is pressure generated from the ideal gas law

$$P_{\text{gas}} = nkT \tag{2.2.3}$$

where $n = N/V$ is the particle number density, $k = 1.38 * 10^{-23}$ $\text{kgm}^2\text{s}^{-2}\text{K}^{-1}$ is Boltzmann's constant, and T is the temperature in Kelvin [5]. This can be rewritten when allowing $n = \rho/\bar{m}$, where $\bar{m}$ is the average mass of a gas particle, and $\mu = \bar{m}/m_{\text{H}}$, where $m_{\text{H}} = 1.67 * 10^{-27}$ kg is the mass of the hydrogen atom,

$$P_{\text{gas}} = \frac{\rho kT}{\mu m_{\text{H}}}. \tag{2.2.4}$$

Since photons have momentum via the de Broglie wavelength, $\lambda = h/p$, pressure is also generated from radiation. This can be derived from blackbody radiation and expressed as

$$P_{\text{rad}} = \frac{1}{3} aT^4 \tag{2.2.5}$$

where $a = 4\sigma/c = 7.565 * 10^{-16}$ $\text{Jm}^{-3}\text{K}^{-4}$ [5]. The gas and radiation pressure, with the exception of the insignificant degeneracy pressure in a main sequence-like star, make up the total pressure in a star

$$P_{\text{total}} = \frac{\rho kT}{\mu m_{\text{H}}} + \frac{1}{3} aT^4. \tag{2.2.6}$$

Figure 2 below helps visually represent the hydrostatic equilibrium balance.

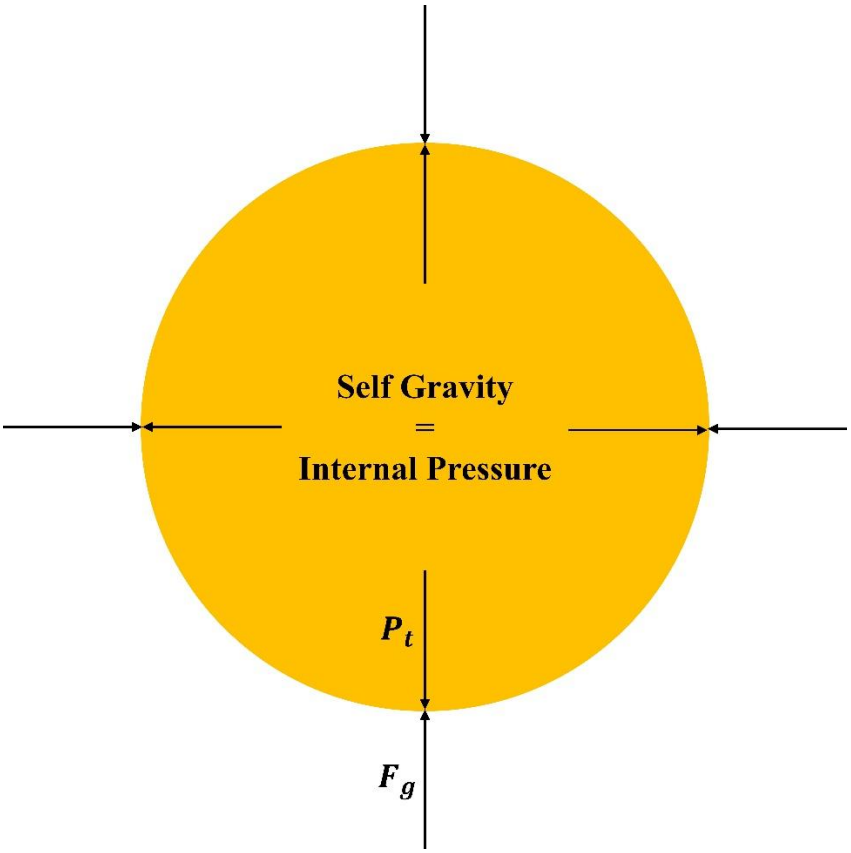


Figure 2: Hydrostatic Equilibrium in a pre-MS star.
This is when the inherent attractive gravitational force equals the outward total pressure, made up of Ideal Gas and Radiation pressures.

2.2.2 Evolutionary Stages

All stars have different intrinsic physical and chemical properties that define their identity. The fundamental ones are mass, size, metallicity, luminosity, and temperature. Metallicity is the percent composition of elements heavier than helium and therefore has a great effect on the fusion processes that occur inside a star. Luminosity is power (energy per time), and is expressed numerically as

$$L_* = 4\pi R_*^2 \sigma T^4 \tag{2.2.7}$$

where $\sigma = 5.67 * 10^{-8}\ \mathrm{Wm^{-2}K^{-4}}$ is the Stefan-Boltzmann constant. A star's luminosity can be plotted against its temperature (with reversed magnitude) in what is called a Hertzsprung-Russell (HR) diagram. This is used to show the evolutionary tracks of any possible star. A star is placed into one of five different categories based on where it falls on the HR diagram: pre-main sequence, main sequence, red giant, supergiant, and white dwarf.

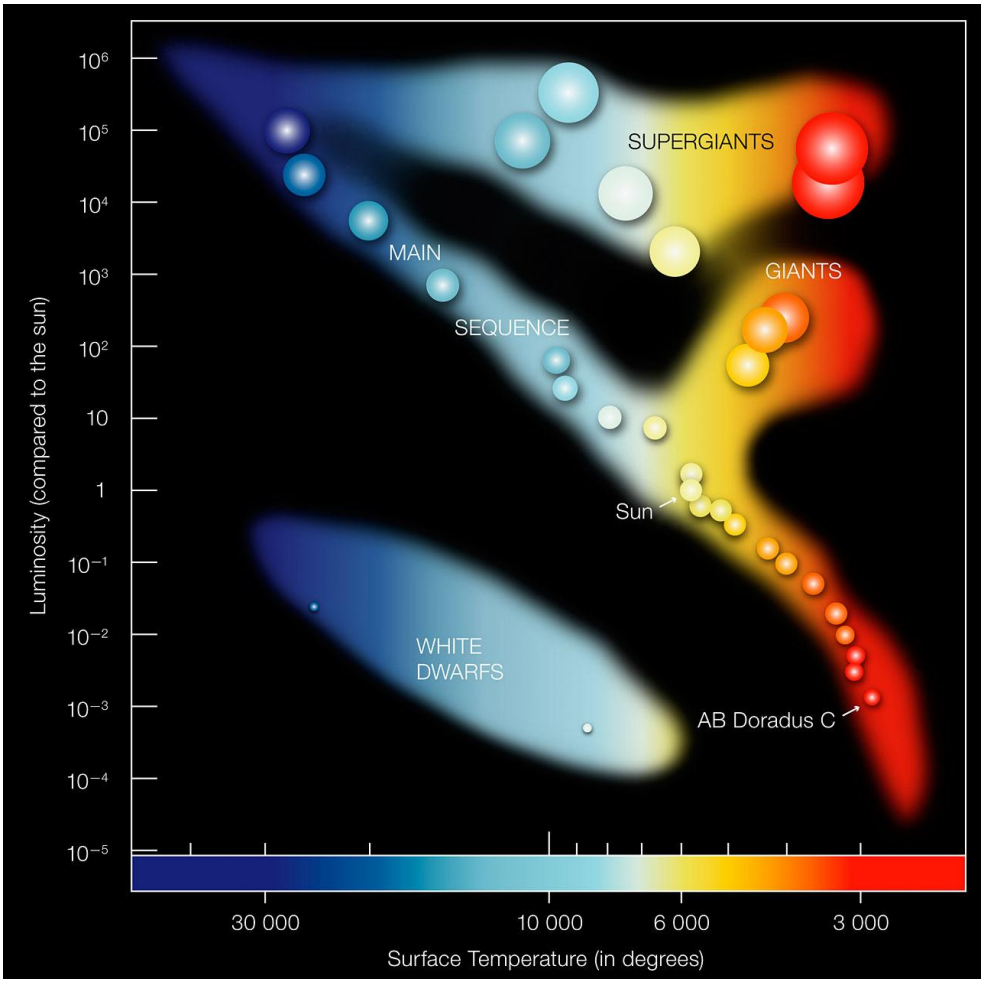


Figure 3: An HR diagram showing all the different possible evolutionary tracks for a star [7].
A star begins its evolutionary track on the bottom right of this plot, the pre-main sequence. The Sun is in the main sequence, where stars spend most of their lifetime. Depending on the mass of the star, evolution will continue to giants, supergiants, white dwarfs, or black holes.

A pre-main sequence (pre-MS) star is in the stage after being a protostar (when the star is being formed) that has begun to contract and heat up but has not yet started fusing hydrogen into helium. A main sequence (MS) star is one that fuses hydrogen into helium through a process called the proton-proton (PPI, PPII, PPIII) chain, expressed as the chemical reactions in Figure 4 below [5].

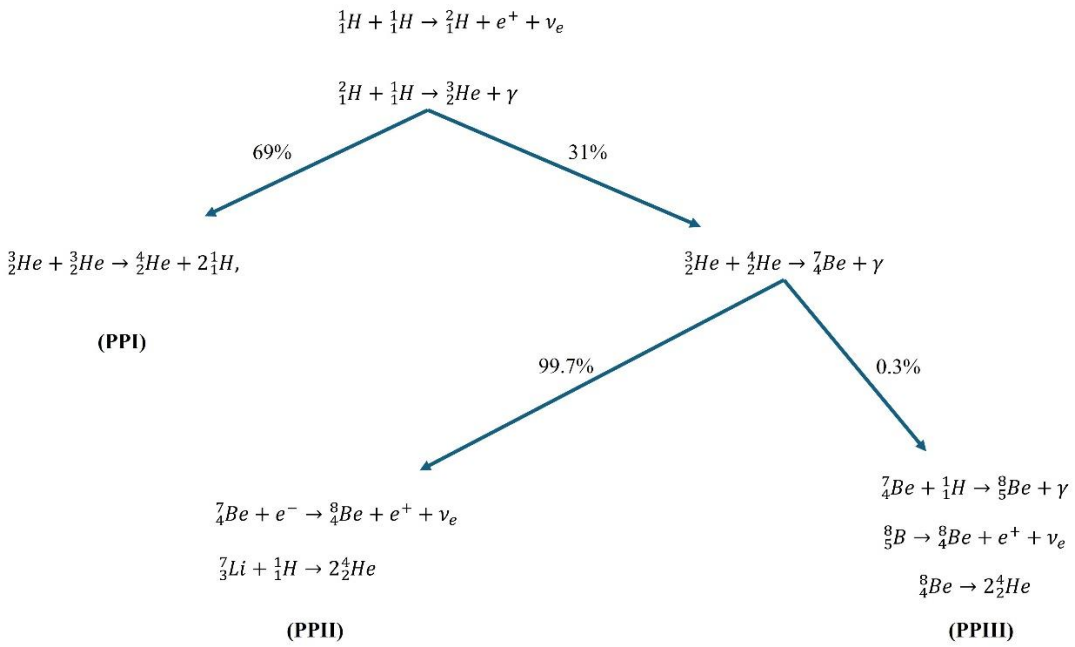


Figure 4: The three possible stages of the pp chain.
H is hydrogen, He is helium, Be is beryllium, Li is lithium, e^+ is a positron, ν_e is a neutrino, and γ is a photon [5]. The percentages represent the probability of occurring in the core of the Sun. Each stage conserves charge and lepton number between both sides of the chemical equation arrow.

MS stars make up 80-90% of the stars on the H-R diagram [5]. MS stars are the most common stars to study computationally due to there being more empirical data to compare with. The Sun is an MS star, which can be seen in Figure 2. The carbon-nitrogen-oxygen (CNO) cycle is another method of producing helium in the core of MS stars but is primarily used in stars at least twice as massive as the Sun due to its dependence on the presence of carbon in the core of the star [5]. The star studied in this project is classified as a pre-MS star and is about 25,000 years away from hydrogen burning compared to its 60,000-year age. Although MS stars are the most prevalent, pre-MS stars are still relevant because they will evolve to MS stars throughout their time in stellar clusters.

Once a star has fused all the hydrogen in its core to helium, it is no longer an MS star but is on its way to becoming a red giant (RG). Once this criterion is met, the gravitational force outweighs the radiation pressure from Equation 2.2.2, causing the core of the star to begin collapsing. However, the temperature begins to rise in the outer layer (a shell around the core), the shell begins fusing hydrogen to helium and ends up producing more energy output than the star did during the MS [5]. This energy output causes the envelope to expand and the surface

temperature to decrease. At this point, the star begins fusing helium to carbon in its core via the triple alpha process, classifying it as an RG [5]. The triple alpha process is expressed as

$$^{4}_{2}He + {}^{4}_{2}He \rightleftharpoons {}^{8}_{4}Be \qquad (2.2.8A)$$

$$^{8}_{4}Be + {}^{4}_{2}He \rightarrow {}^{12}_{6}C + \gamma \qquad (2.2.8B)$$

where C is carbon. MS stars greater than or equal to 8-10 $M_{\odot}$ will be classified as supergiant stars.

When MS or RG stars $\lesssim 8\ M_{\odot}$ reach the end of their life, their outer layers will be shed (leaving behind a planetary nebula), leaving its naked core, known as a white dwarf. This signals the end of a star's life.

2.2.3 Globular Clusters

Most collisions between stars and BHs will occur in areas with high number density of stars, this being stellar clusters. Because of this, most wave signals that indicate collisions will be from these stellar clusters since the probability of collision is proportional to the number density of stars in a region. A globular cluster is a specific type of stellar cluster that is a nearly spherical collection of thousands of stars held together by their gravitation, and forms through the collapse of a molecular cloud [5]. Because of their birth from the same cloud, all the stars form with very similar compositions, and therefore, the Vogt-Russell theorem suggests that the differences in evolutionary states between them are solely due to their initial mass [5]. The age of the cluster affects the metallicity of its contents. An older cluster formed when there were fewer heavy elements in the universe, causing stars to be formed with lower metallicities. These clusters will also be at the far edges of the universe because of the universe's constant expansion.

According to research done by Wirth et al., the stellar formation period in globular clusters should be completed within 3.5-10 Myr [8]. For a BH of $30\ M_{\odot}$ in a globular cluster like mine, its progenitor should be at least $\sim 80\ M_{\odot}$ [9]. Portinari et al.'s data shows that this progenitor has a stellar lifetime of 3-4 Myr; therefore, this should fit into the expected duration of stellar formation in a globular cluster. This information provides evidence that the collision in scenario #2, discussed later, is possible and likely.

For a star in a dense star cluster core, the typical collision timescale is on the order of the cluster lifetime, which motivates a high probability of all stars in a cluster being affected by a collision at some point in their life [10]. Fregeau et al. discusses that collisions between stars and BBHs in dense globular clusters and open clusters is motivated to happen frequently [10]. Due to the complexity of globular clusters, research on their contents is prevalent.

2.3 Black Holes

Not everything in space can be seen with the naked eye or through a telescope, and sometimes not even through electromagnetic wave signals. Black holes (BHs) are points in space with infinite density where the gravity is so strong that nothing, not even electromagnetic waves, can escape it. BHs are characterized by their mass, spin, and charge. The only way to detect a BH is through detecting electromagnetic waves from an accretion disk (a disk of stellar matter that was stripped onto the BH) or detecting gravitational waves (GWs) through a laser interferometer.

2.3.1 Schwarzschild Radius

For an object to become a BH it must collapse to the size of its Schwarzschild Radius, R_{s}. This is the radius of the object where the escape velocity, v_{escape}, of another object leaving its surface equals the speed of light, meaning that electromagnetic waves, and therefore light, cannot escape from inside this radius. The actual derivation requires knowledge of general relativity as the escape velocity reaches the speed of light; however, a classical relationship can be used to reach a similar conclusion. First, find the escape velocity by using conservation of energy, where the final energy, where the object is gravitationally unbound, is zero

$$E_{\mathrm{initial}} = E_{\mathrm{final}}$$

$$K_{\mathrm{initial}} + U_{\mathrm{initial}} = 0$$

$$\frac{1}{2}mv^2 + \left(-\frac{GMm}{R}\right) = 0$$

$$v_{\mathrm{escape}} = \sqrt{\frac{2GM}{R}}, \tag{2.3.1}$$

where M is the mass of the first object, R is the radius of the first object, and m is the mass of the second object escaping the first object [5]. As shown, the escape velocity does not depend on the mass of the second object. Then, set Equation 2.2.1 equal to the speed of light, c, to get

$$v_{\text{escape}} = \sqrt{\frac{2GM}{R}} = c$$

$$R_s = \frac{2GM}{c^2} \tag{2.3.2}$$

where M is the mass of the BH, in this case [5]. This is also known as the distance from the center of the BH, known as the singularity, to the outer edge of the BH, known as the event horizon. The event horizon is the point where observers cannot detect any more information about the BH; however, other techniques can be used to learn information about BHs, as discussed in Section 2.4. The components of a BH are shown in Figure 5 below.

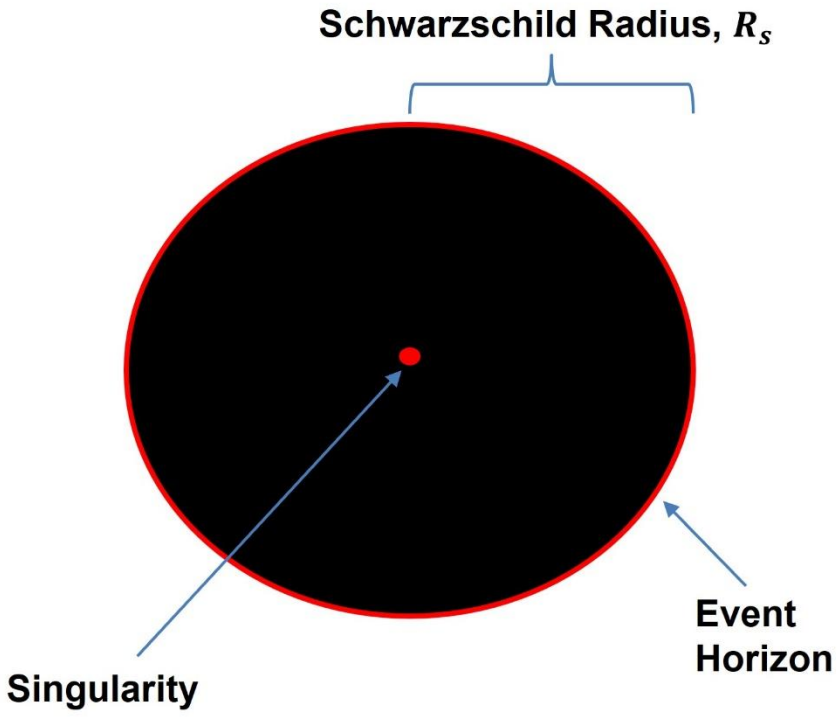


Figure 5: The components of a BH.
The singularity (the center), the event horizon (the outer edge) and the Schwarzschild Radius, R_s, are all explained above.

2.3.2 Tidal Force and Tidal Radius

Resulting from the negative sign in Equation 2.1.3, objects are gravitationally attracted to each other. Since Equation 2.1.3 depends on the distance-squared between two objects, distance will have a greater effect on this force compared to the masses of the objects, causing the closer side of an object being attracted to the other object before the farther side. This leads to stretching depending on the distance between and masses of the two objects. The force behind this phenomenon is known as the tidal force, F_{t}, and the action is known as tidal attraction. This is seen between the Earth and the Moon with the Moon being tidally locked to the Earth; however, due to the mass difference and distance between the two, neither the Moon nor the Earth are torn apart because the tidal force is not large enough to do so.

In a star-BH interaction, to derive the tidal force, picture the forces of a particle on the surface of the star closest to the BH, and another particle at the center of the star. Both particles have mass m. Subtract the gravitational force between the surface of the star and the BH, $F_{\mathrm{g,s}}$, by the center of the star and the BH, $F_{\mathrm{g,c}}$

$$F_{\mathrm{t}} = F_{\mathrm{g,s}} - F_{\mathrm{g,c}}$$

$$F_{\mathrm{t}} = G\frac{M_{\mathrm{BH}}m}{(r-R_*)^2} - G\frac{M_{\mathrm{BH}}m}{r^2}.$$

To solve this, a Taylor Expansion can be used,

$$F_{\mathrm{g,s}} \to f(r-R_*) \approx f(r) + f'(r) * (-R_*) + \cdots \tag{2.3.3}$$

$$F_{\mathrm{t}} = G\frac{M_{\mathrm{BH}}m}{r^2} + 2G\frac{M_{\mathrm{BH}}mR_*}{r^3} - G\frac{M_{\mathrm{BH}}m}{r^2}$$

$$F_{\mathrm{t}} = 2G\frac{M_{\mathrm{BH}}mR_*}{r^3}, \tag{2.3.4}$$

where M_{BH} is the mass of the BH, M_* is the mass of the star, R_* is the radius of the star, and r is the distance between the center of mass of the star and the BH [5]. As shown by Equation 2.3.4, the tidal force has a distance-cubed dependence, making this force robust as the star approaches close to the BH.

The proximity of a star to a BH where it is destroyed can be quantified by setting the tidal force of the star equal to the gravitational force of the star, as portrayed in Figure 6 below.

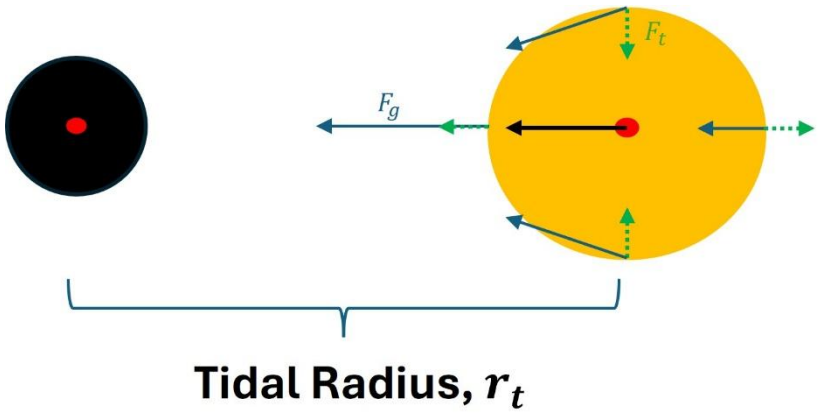


Figure 6: The tidal radius, r_t.
This is the separation distance where a star will be destroyed by a BH. F_g is the gravitational force from the BH on the star and F_t is the tidal force of the BH on the star. The green dashed arrows show the direction of F_t at different points in the star. Because of this, the star will be squished, with the top and bottom points compressing to the center, and the close and far points stretching outward. The black arrow originating from the center of the star shows the horizontal component of the triangle that would be made from the F_t and F_g vectors at the top and bottom of the star. This vector equals $F_g - F_t$.

With these forces set opposite but equal, and dropping the multiplicative factor of 2, solve for r to derive an expression for the tidal radius [5]

$$F_t = -F_g$$

$$2G\frac{M_{BH}mR_*}{r^3} = G\frac{M_*m}{R_*^2}$$

$$r_t \approx R_*\left(\frac{M_{BH}}{M_*}\right)^{\frac{1}{3}}. \qquad (2.3.5)$$

It is useful to note that the above relation between the tidal and gravitational forces used in Equation 2.3.5 is limited to non-solid objects because the rigidity of solid objects lacks the deformative nature of, for example, liquid.

2.3.3 Tidal Disruption Events

When a star approaches a BH within a proximity of 1 r_t, the star will be destroyed in a tidal disruption event (TDE). During this, the BH will gravitationally attract stellar mass toward it through the process of accretion, placing it onto its outer layer in an accretion disk. Accretion

disks are one of the few ways (gravitational lensing being another method) to visualize a BH since any mass or radiation that enters the BH past the event horizon will be lost due to the intense gravity.

Within a proximity of about 1-2 r_t, the star will be partially destroyed in a partial tidal disruption event (PTDE). This causes layers of the star to be stripped onto the accretion disk, and the resulting star being elliptically bound to the BH.

The spin of the accretion disk can be constrained by monitoring both electromagnetic wave and GW signals, which helps us learn about the characteristics of BBHs from before and after TDEs, described further in Section 2.4.2.

2.3.4 Binary Black Holes

With the abundance of stars and BHs in stellar clusters, there are plenty of star-star, star-BH, and BH-BH interactions; however, not all these results in immediate collisions where one or both objects are destroyed or merged. Instead, due to orbits as discussed in Section 2.5.2, stars and BHs can be locked co-orbiting each other in what is known as a binary. For this research, I am focusing on binary black holes (BBHs), meaning two BHs are co-orbiting each other. There are three popular methods to form a BBH, which will be discussed below, with Figure 7, Figure 8, and Figure 9 from Mandel and Farmer (2022) [11].

The first method is dynamical assembly in dense stellar clusters, which is the method in which the BBHs in the scenarios studied here were formed. This process involves two distinct BHs who are introduced to each other by an array of “matchmakers” (other cluster members) [11]. Since the BHs are the densest objects in their vicinity, they will be apt to move to the center of the cluster, where they may involve themselves in three-body interactions, possibly leaving behind a binary [11]. If the orbital speed of the binary is greater than the typical speed of stars in the cluster (this is known as a “hard binary”), then subsequent interactions with the “matchmakers” will tighten the binary [11]. Meanwhile, soft binaries will be disrupted by the “matchmakers” [11].

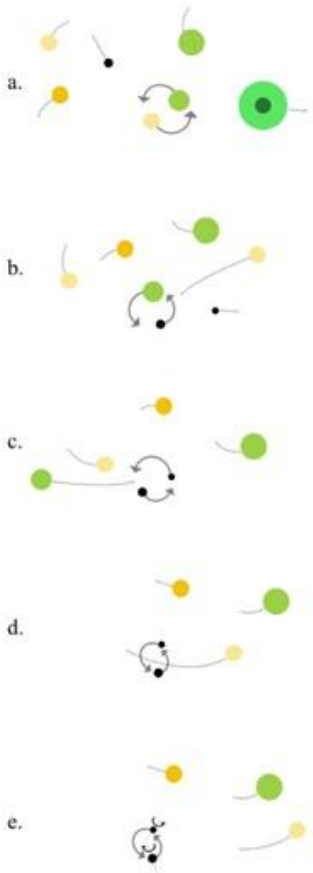


Figure 7: BBH formation through dynamical assembly.
The black dots are BHs, and the colored dots are differently massed stars. Step a. assumes two BHs formed in a globular cluster. A sufficient three-body interaction between a stellar binary and a BH will cause an exchange between one of the stars and the BH, leaving behind a star-BH binary. This happens again to form a BBH. As the BHs are the densest objects in the cluster, they will be apt to segregate toward the center of the cluster as shown in step b. Steps c. and d. show how greater BBH orbital speed leads to the creation of a hard binary. The BBH will then be hardened enough to lead to a merger, producing GWs, as shown in step e. This is expected to have $\langle \chi_{\text{eff}} \rangle \approx 0$, but research by Kıroğlu et al. shows this may not be the case [4]. All credit for this figure is to Mandel and Farmer (2022) [11].

The second method is with isolated massive stellar field binaries, which involves two stars born in a binary. The heavier of the two stars (the primary star) completes its MS lifetime first (stellar evolution is discussed further in Section 2.4) causing its core to contract and its outer layers to expand past the equipotential surface known as the Roche Lobe [11]. For a close enough binary, the primary star will transfer mass to the secondary star [11]. The primary star eventually loses its entire envelope and is left behind as a naked helium-burning star, known as a Wolf-Rayet star, eventually collapsing to a BH [11]. Hundreds of years later, this process repeats but with the secondary star as the new primary star, and eventually there are two BHs left in a binary [11].

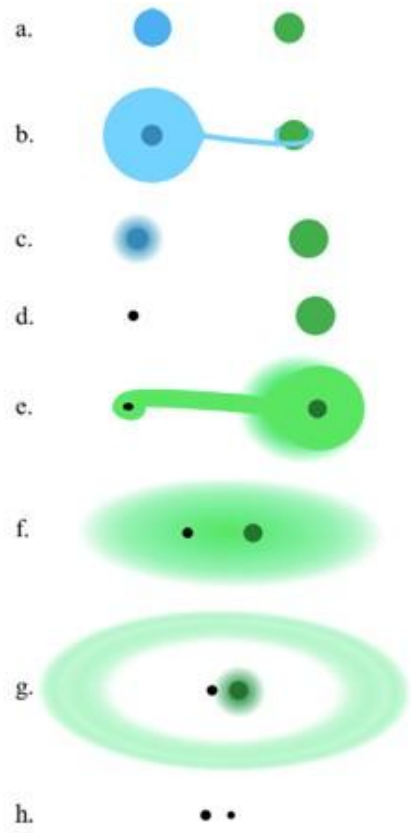


Figure 8: BBH formation through isolated binary evolution.
The blue dot represents the primary, more massive star. The green dot represents the secondary, less massive star. Step a. assumes two stars of different properties born in a binary. Step b. shows the primary star expanding and the secondary star accreting its mass. Step c. shows the primary star as a Wolf-Rayet star. Step d. shows the primary star becoming a BH. Step e. shows the reverse process, as the secondary star expands, and mass is accreted onto the BH (the primary). Step f. shows an inspiral due to drag force from the common envelope. Step g. shows the secondary as a Wolf-Rayet star, with further evolution into a BBH in step h. This leads to $\langle \chi_{\text{eff}} \rangle \gtrsim 0$. All credit for this figure is to Mandel and Farmer (2022) [11].

The third method is chemically homogenous evolution, which involves stars in a binary. If the binary is tight enough where each star covers a significant fraction of the Roche Lobe, then tidal energy is dissipated, and the stars become tidally locked (i.e. the axis rotation period is equal to the orbital period) [11]. Due to significant temperature gradients, mixing of chemical species in the stars is increased, causing the transport of hydrogen to the core and helium out of the core [11]. This happens until nearly all the hydrogen in the star is fused into helium. Because of this, the stars will behave like a Wolf-Rayet star, eventually collapsing into BHs. If the metallicity is sufficiently low that the wind-driven mass loss will not widen the binary (which would lead to loss of chemical homogeneity), then the binary can avoid mass transfer, allowing the BBH to be formed [11].

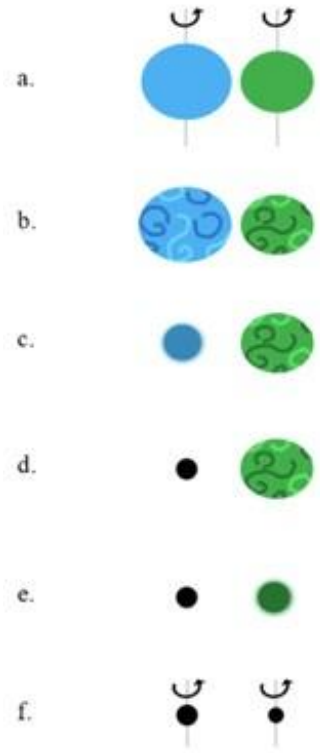


Figure 9: BBH formation through chemically homogenous evolution.
Step a. shows two stars in a binary becoming tidally locked. Step b. shows temperature gradients causing mixing, leading to nearly all hydrogen being fused into helium. Steps c-f show the leftover Wolf-Rayet stars eventually collapsing into BHs. This leads to $\langle \chi_{\text{eff}} \rangle \gtrsim 0$. All credit for this figure is to Mandel and Farmer (2022) [11].

These formation channels help to motivate why positive χ_{eff} values are seen in LIGO data. Figure 8 and Figure 9 show stars initially in a binary that end up forming a BBH. The BH spins are more likely to be aligned in these scenarios, causing a strong BBH spin in that direction. This strong alignment could be a cause for positive χ_{eff} values after a stellar collision with the BBH, further discussed in Section 2.4.2. However, since the scenarios I am researching were formed via dynamical assembly, I am searching for reasons that cause positive χ_{eff} for that formation channel, which is supported by Kıroğlu et al [4].

2.3.5 Interaction Timescales

It is important to quantify the timescales of related astrophysical processes to determine whether they can coexist. Due to its size and gravitational boundness, a globular cluster's contents of stars and BHs will inevitably interact with each other. The encounter timescale, t_{enc}, is the time between each subsequent encounter with another object, and is calculated by

$$t_{\text{enc}} = (n\Sigma_{\text{bs}}\sigma_{\text{v}})^{-1}, \tag{2.3.6}$$

where n is the number density of stars in the cluster, Σ_{bs} is the cross section for binary-single encounters, and σ_v is the central velocity dispersion, which can be thought of as an average velocity for the celestial bodies studied. Σ_{bs} is found by using the circular cross section of a sphere and using $r = a$, as any object that enters the semi-major axis distance of a BBH will likely be trapped in its orbit [12]. A gravitational focusing factor, F, must also be used to consider how spacetime is warped around BHs,

$$\Sigma_{\mathrm{bs}} = \pi a^2 F \tag{2.3.7}$$

$$F = 1 + \frac{G M_{\mathrm{tot}}}{a v_\infty^2}. \tag{2.3.8}$$

From this, using information from section 3.1 and an assumption of $\sigma_{\mathrm{v}} \approx v_\infty = 16.5 \frac{km}{s}$ for these simulations, where v_∞ is the velocity of the star infinitely away from the BBH, t_{enc} is estimated to be

$$F = \left(1 + \frac{6.67 * 10^{-11} \frac{\mathrm{m}^3}{\mathrm{kg} * \mathrm{s}^2} * 60\ \mathrm{M}_\odot * 1.989 * 10^{30} \frac{\mathrm{kg}}{\mathrm{M}_\odot}}{0.5\ \mathrm{AU} * 1.496 * 10^{11} \frac{\mathrm{m}}{\mathrm{AU}} * \left(16500 \frac{\mathrm{m}}{\mathrm{s}}\right)^2} \right)$$

$$t_{\mathrm{enc}} = \left(\frac{8 * 10^5\ \mathrm{stars}}{\frac{4}{3}\pi \left(1\ pc * 3.086 * 10^{16} \frac{\mathrm{m}}{\mathrm{pc}}\right)^3} * 16500 \frac{\mathrm{m}}{\mathrm{s}} * \pi \left(0.5\ \mathrm{AU} * 1.496 * 10^{11} \frac{\mathrm{m}}{\mathrm{AU}}\right)^2 * F \right)^{-1}$$

$$t_{\mathrm{enc}} \approx 43\ \mathrm{Myr}$$

Extracted from this equation, the time between encounters relies on how many stars are in the cluster, the size of the cluster, the size of the star and BBH, and the velocities of the star and BBH. For scenario #2, the BBH will have a subsequent encounter on the order of 43 Myr [4].

It is also important to recognize that a subsequent encounter before the BBH is allowed to inspiral is undesirable, as the data from the first encounter may become meaningless due to further perturbation. The inspiral timescale, t_{GW}, is the time it takes for a BBH to collapse its orbit and the BHs merge. This can be calculated using an equation found by Peters, relating the

change in semi-major axis, da, to the change in eccentricity, de, in conjunction with other equations used by Peters [13],

$$\left\langle \frac{da}{de} \right\rangle = \frac{12}{19}\frac{a}{e}\frac{\left(1+\frac{73}{24}e^2+\frac{37}{96}e^4\right)}{(1-e^2)\left(1+\frac{121}{304}e^2\right)} . \tag{2.3.9}$$

For my simulations, initially I want $t_{\mathrm{enc}} < t_{\mathrm{GW}}$ since I do not want the BBH to inspiral before interacting with the star. However, after the interaction with the star, I want $t_{\mathrm{GW}} < t_{\mathrm{enc}}$ so that the BBH does not interact with another star. If this goes to plan, then I will be able to find direct causes of positive χ_{eff} values.

2.4 Gravitational Waves

Looking back at Section 2.1, gravity can be represented as a force of one particle on another particle through Equation 2.1.1. However, gravity can be thought of as a field as well. For example, if the Sun approaches a 100 $M_\odot$ BH, the Sun will begin to move closer to the BH because the Sun is in the BHs stronger gravitational pull, making the Sun enter the BH's gravitational field. A common metaphor is to think of space as a fabric and when a more massive object is placed in that fabric, it stretches the fabric more, causing a less massive object to "fall" toward the more massive object.

Albert Einstein's general theory of relativity predicts the existence of GWs, which are ripples through the spacetime fabric that are outputted when an object moves through the fabric. In other words, when the distribution of a system's mass changes, the resulting adjustment to the surrounding spacetime curvature may propagate outward as a GW which carries energy and angular momentum [5]. This happens in BBHs as they are orbiting about each other. General relativity states that the release of GWs is what causes orbits to lose energy and angular momentum and spiral inward [5].

2.4.1 Laser Interferometers for Observing Gravitational Waves

Since these GWs translate throughout the universe, they will reach Earth, meaning that we can detect them. The first direct observation of GWs was in 2015 by the Laser Interferometer

Gravitational Wave Observatory (LIGO). LIGO has two facilities, one in Livingston, Louisiana and the other in Hanford, Washington. Both facilities have large laser interferometers which split a laser beam and then recombine it, measuring the interference in the recombined beam. This is known as a Michelson Interferometer and is shown in Figure 10. An initial laser beam is sent toward a beam splitter which splits the beam, sending one part continuing straight and the other part perpendicular. These parts are two arms, where each laser enters a 4 kilometer-long Fabry-Perot cavity: an optical cavity made from two parallel mirrors which only let waves through if they are in resonance with it [14]. The purpose of this cavity is to measure specific frequencies, as the only interference that is wanted is from GWs. Once the lasers meet this criterion, they are recombined and measured for interference [15].

One problem is there needs to be a power supply closer to 750 kilowatts, but LIGO's laser enters the interferometer at 40 watts. To fix this, a power recycling mirror is used. This is used as a one-way mirror, letting laser light into the interferometer arms, but reflecting the light that is attempting to travel out of the arms back into the arms. Therefore, this strengthens the laser beams by recycling the energy that has already been used. A more powerful laser beam results in sharper interference fringes, allowing both the detection of weaker GW signals and easier detection of stronger GW signals [15].

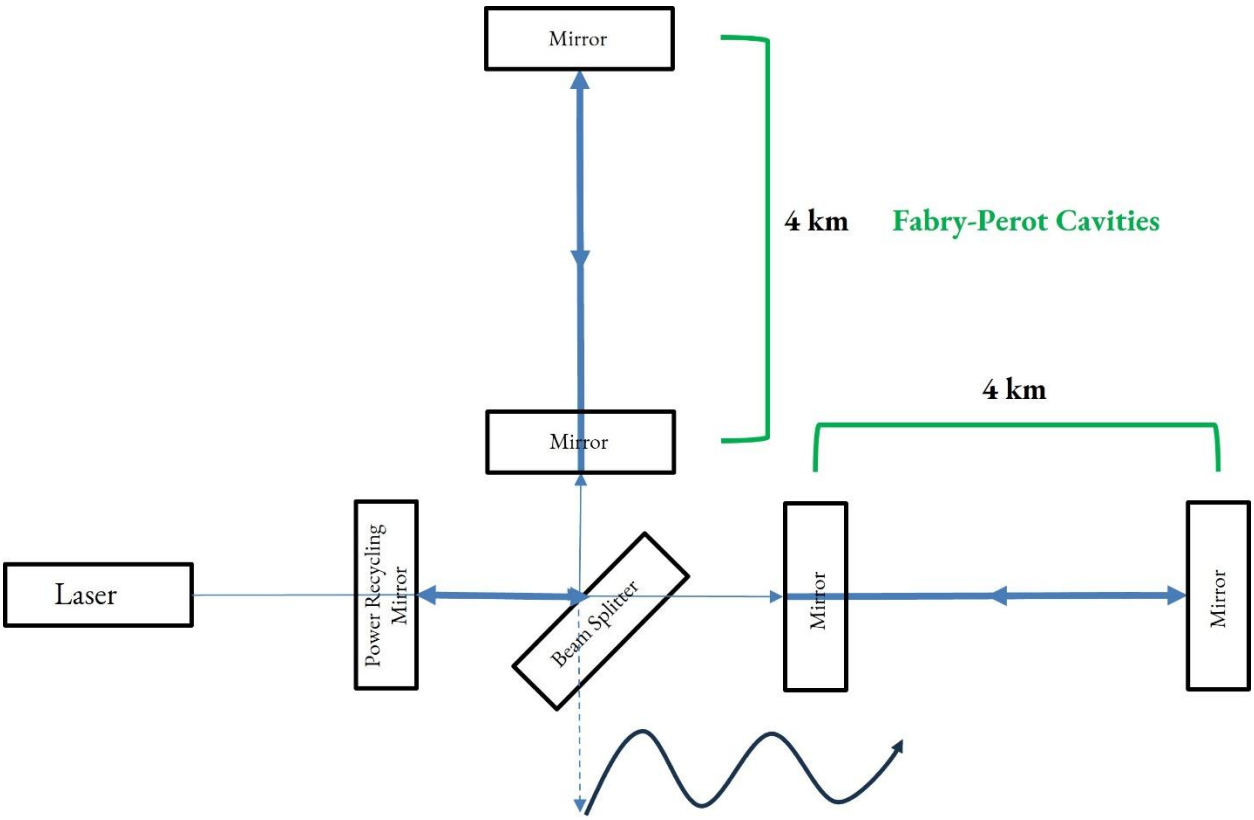


Figure 10: A basic blueprint of the Michelson Interferometer used at LIGO and other observatories [15]. GWs are found based on interference patterns detected in lasers after the beams are split and then recombined. The power recycling mirror reflects light that has not been fully transmitted through the beam splitter, as optics and quantum mechanics do not allow 100% transmission.

LIGO is not the only active laser interferometer for observing GWs. The three other active detectors are the Kamioka Gravitational Wave Detector (KAGRA), located in Japan; Virgo, located in Pisa, Italy; and GEO600, located in Hannover, Germany. The Laser Interferometer Space Antenna (LISA) is a space-based detector that plans to be active by 2034. LISA is special because due to it being in space, it will be able to detect more GWs than have been possible with the interferometers on Earth.

2.4.2 The Dimensionless Spin Parameter, χ_{eff}

The dimensionless spin parameter, χ_{eff}, represents the total mass-weighted BH spin components in the direction of the BBH orbital angular momentum. This parameter, along with BH masses and orbital eccentricity, helps quantify BBH formation channels [1] and can be calculated from LIGO data. The equation is represented by a dot product as

$$\chi_{\text{eff}} = \frac{M_{\text{BH1}}\,\vec{S}_{\text{BH1}} + M_{\text{BH2}}\vec{S}_{\text{BH2}}}{M_{\text{BH1}} + M_{\text{BH2}}} \cdot \hat{L}_{\text{BBH}}, \tag{2.4.1}$$

where M_{BH1} and M_{BH2} are the masses of BH #1 and BH #2, $\vec{S}_{\text{BH1}}$ and $\vec{S}_{\text{BH2}}$ are the spin vectors of BH #1 and BH #2 in units of angular momentum, and $\hat{L}_{\text{BBH}}$ is the dimensionless unit vector representing the direction of the BBH orbital angular momentum. Although it may not seem this way in equation 2.4.1, χ_{eff} is dimensionless when normalized with $c = G = 1$, which is the same normalization used in *StarSmasher*. For the dynamical assembly method of forming a BBH as explained in Section 2.3.4, χ_{eff} is expected to be centered around zero because they are formed through a series of chaotic, random interactions [1]; however, for the isolated massive stellar field binary formation channel, χ_{eff} is seen to be more positive ($\vec{S}_{\text{tot}}$ and $\hat{L}_{\text{BBH}}$ in the same direction) because of the similar evolution between both BHs in the same system [1].

The spin of a BH is calculated by determining a change in the BH mass after accretion. Lopez et al. (2019) states this can be calculated by

$$S(M_{\text{BH},f}) = \left(\frac{2}{3}\right)^{\frac{1}{2}} \left(\frac{M_{\text{BH}}}{M_{\text{BH},f}}\right) \left\{4 - \left[18\left(\frac{M_{\text{BH}}}{M_{\text{BH},f}}\right)^{2} - 2\right]^{\frac{1}{2}}\right\}, \tag{2.4.2}$$

where $M_{\text{BH,f}}$ is the final BH mass (specifically, $M_{\text{BH,f}} = M_{\text{BH}} + M_{\text{disk}}$, with $M_{\text{disk}} = fM_{*}$, where f is the fraction of stellar mass accreted). As shown in Figure 11, $\chi_{\text{eff}} = 1$ represents the BH spins being parallel to the BBH orbit, $\chi_{\text{eff}} = 0$ represents a perpendicular relationship, and $\chi_{\text{eff}} = -1$ represents an anti-parallel relationship.

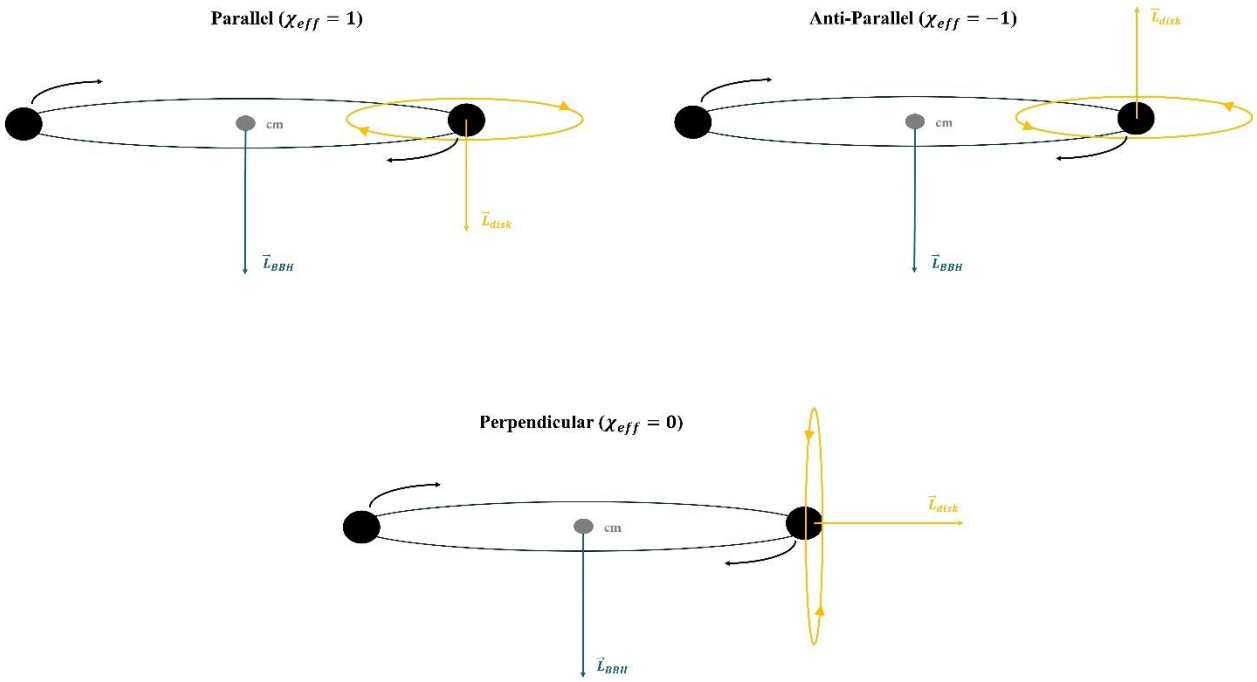


Figure 11: The three different extreme relationships between $\vec{L}_{\mathrm{BBH}}$ and $\vec{L}_{\mathrm{disk}}$ to set boundary conditions on χ_{eff} values (from -1 to 1).
The yellow represents stellar mass in an accretion disk around a BH (this is simplified, as there can be accretion disks around both BHs).

We use post-processing code (discussed further in Section 3.5) to calculate χ_{eff} from *StarSmasher* output by implementing Equations 2.4.1 and 2.4.2. Here, cm is the center of mass between the two BHs (which allows a circular orbit in the figure due to a central cm), and $\vec{L}_{disk}$ is the angular momentum of the accretion disk of one of the BHs (there can be disks about both BHs, but this is not visualized), which is a physical representation of the accreted mass that alters the spin of the BH, explained by Equation 2.4.2.

2.5 Rotations and Orbits

Introductory physics teaches the law of angular momentum and often provides the example of a figure skater pulling their arms in leading to them rotating faster. Introductory chemistry teaches the basic thought of electrons orbiting the nucleus. In astrophysics, similar rotations and orbits are necessities for processes such as our solar system, moons, galaxies, binary systems, and lots more.

2.5.1 The Six Degrees of Freedom of Orbits

There are lots of methods to orient a rotating system that will provide unique results. These methods are expressed as degrees of freedom: Values that are free to vary in a system. There are six degrees of freedom of orbit: Semi-major axis, eccentricity, argument of periapsis, inclination, longitude of the ascending node, and true anomaly. For reference, see Figure 12 and Figure 13 below.

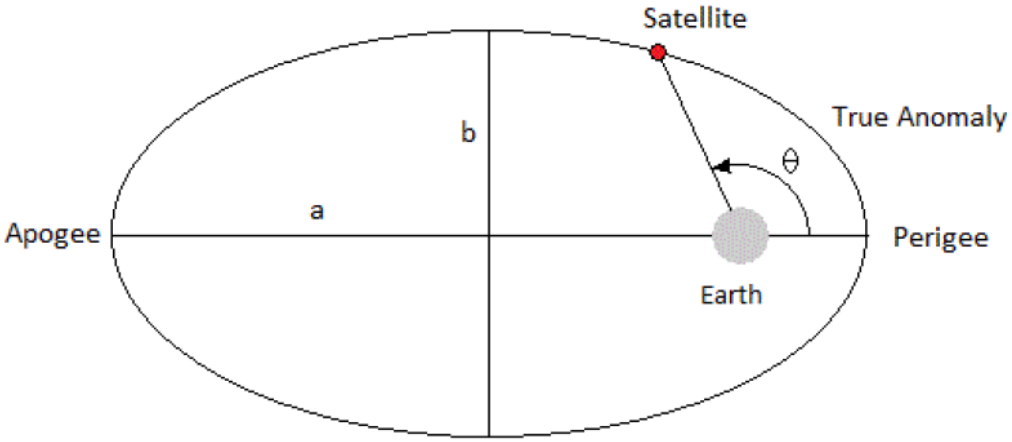


Figure 12: The semi-major (a) and semi-minor (b) axes, apoapsis and periapsis, and true anomaly (ν) [16].
The suffix -gee is used here for representing the orbit of a satellite or a moon, however, the suffix -apsis is used for more general scenarios (e.g. apoapsis and periapsis).

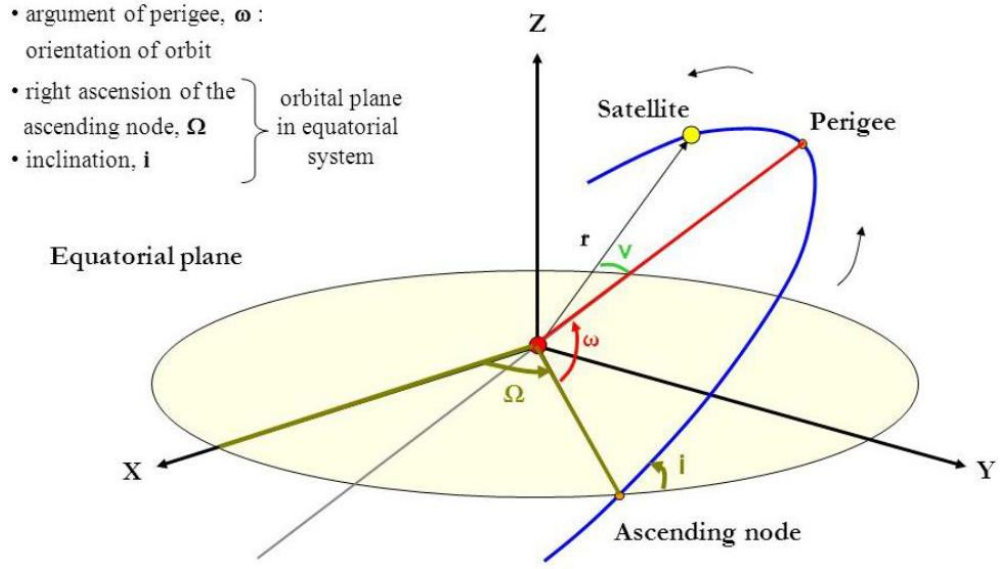


Figure 13: The argument of periapsis (ω), inclination (i), longitude of the ascending node (Ω), and true anomaly (ν).

This figure helps to visualize these orbital elements with the cartesian axes, as well as the ascending node: The point where the orbit rises through the equatorial plane [16]. Rather than a satellite orbiting the Earth, picture this as a BH orbiting another BH (therefore, a BBH).

The semi-major axis, a, is the distance from the center of an ellipse to the edge of the longest side. This, along with the semi-minor axis, b, are used to calculate the eccentricity, e, of an orbit, or how circular an orbit is (explained further in Section 2.5.2)

$$e = \sqrt{1 - \frac{b^2}{a^2}}. \tag{2.5.1}$$

The first rotation is the argument of periapsis, ω: The angle difference of the orbit away from the reference (in this case, x) direction (rotated about the z-axis).

The second rotation is the inclination, i: The angle difference of the orbit from the equatorial plane (rotated about the y-axis).

The third rotation is the longitude of the ascending node, Ω: The angle difference of the ascending node from the reference (x) direction (rotated about the z-axis). This rotation must be done after ω due to the definition of ω's rotation (rotation about the same axis).

The fourth rotation is the true anomaly, ν: The initial angle difference for the orbiting object away from periapsis. This can be thought of as the phase of the orbit, and for star-BBH collisions is therefore dependent on initial distance away the star is from the BBH in our *StarSmasher* dynamical models. Because of this, when aiming to prove the most influential orbital elements on causing collisions, ν is not the best parameter to analyze since it is more dependent on time of the collision rather than the intrinsic properties of the system orientation before the collision.

2.5.2 Circular, Elliptical, Parabolic, and Hyperbolic Orbits

Whether or not an incoming orbit will be bound or unbound after an interaction depends on the eccentricity. Bound orbits include circular and elliptical, with a value $e = 0$ representing a circular orbit and $0 < e < 1$ an elliptical orbit. Qualitatively, for this research, these are two BHs locked in an orbit about one another, very slowly losing energy, eventually inspiralling and merging.

Unbound orbits include parabolic and hyperbolic, with a value $e = 1$ representing a parabolic orbit and $e > 1$ a hyperbolic orbit. A parabolic orbit is the minimum required energy for an object to pass by another object and become unbound from the system, causing its velocity-at-infinity, v_∞, to equal zero. A hyperbolic orbit is any energy greater than this, still causing the object to become unbound from the system, therefore its v_∞ is greater than zero.

2.5.3 Conservation of Angular Momentum

Angular momentum is the rotational form of linear momentum, quantified as

$$\vec{L} = m(\vec{r} \times \vec{v}) \tag{2.5.2}$$

where $\vec{r}$ is the radius vector of rotation, $\vec{v}$ is the velocity vector of rotation, and m is the mass of the object. The criterion for an orbit is bound by the law of conservation of angular momentum

$$\vec{L}_{\text{initial}} = \vec{L}_{\text{final}}. \tag{2.5.3}$$

In a binary system, there are many different sources of angular momentum. Including a third object interacting with the binary adds even more complexity. A star interacting with a BBH will alter the angular momentum of the BBH, which will in turn alter the χ_{eff} value.

2.5.4 Orbital Dynamics

As discussed in section 2.1.2, Newton's universal law of gravitation describes the force present between two massive bodies due to gravity. Under the assumption of a circular orbit, the total energy can be calculated by adding together the kinetic energy, T, and gravitational potential energy, U, to get

$$E = T + U = -\frac{k}{2a}, \tag{2.5.4}$$

where a is the semi-major axis and $k = GM\mu$, with $M = m_1 + m_2$ as the total mass and $\mu = \frac{m_1 m_2}{M}$ as the reduced mass [17].

It can be useful to see how this total energy relates to the eccentricity of an orbit. This is derived from the equation for the path of a particle moving under the influence of a central gravitational force by setting values in the equation to a and e,

$$a = \frac{l^2}{\mu k} \tag{2.5.5}$$

$$e = \sqrt{1 + \frac{2El^2}{\mu k^2}} \tag{2.5.6}$$

where $l = \mu r^2 \dot{\theta}$ is the angular momentum, with $\dot{\theta}$ being the change in the angle between the objects through time [17]. If we assume a circular orbit, then $e_i = 0$, meaning that

$$\frac{2E_i l_i^2}{\mu k^2} = -1. \tag{2.5.7}$$

The distance of closest approach for an orbit, known as the periapsis separation, is found by the following simple relationship between a and e,

$$r_p = a(1 - e). \tag{2.5.8}$$

Solving for a, equation 2.5.8 can be used in conjunction with equation 2.5.4 to plug in to equation 2.5.6,

$$e_f = \sqrt{1 + \frac{-2k}{2a_f} * \frac{l_f^2}{\mu k^2}}$$

$$e_f = \sqrt{1 + \frac{-l_f^2}{a_f \mu k}}. \tag{2.5.9}$$

Equation 2.5.9 gives a relationship between the final eccentricity and both the final BBH angular momentum and semi-major axis. To make this more direct, the angular momentum and semi-major axis can be combined into a composite variable, A,

$$e_f = \sqrt{1 - \frac{A}{\mu k}}. \tag{2.5.10}$$

Taking the instantaneous point where the orbit is at its periapsis ($a = r_p$), equations 2.5.8 and 2.5.9 can be used to prove circular and parabolic properties

$$e_f = \frac{l_f^2 \pm \sqrt{l_f^4 - 4\mu k r_p \left(l_f^2 - \mu k r_p\right)}}{2\mu k r_p}$$

$$e_f = \frac{l_f^2 - l_f^2}{2\mu k r_p} = 0. \tag{2.5.11}$$

$$e_f = \frac{l_f^2 + l_f^2}{2\mu k r_p} = 1. \tag{2.5.12}$$

This proof helps define which variables affect the eccentricity of the BBH after the interaction.

2.5.5 Gravity Assist

Often discussed in the realm of interplanetary travel, gravity assist is a phenomenon that can slingshot a celestial body in the same direction as the motion of another. To save fuel for a mission to and from Mars, a spacecraft aims to use the least energy possible; however, due to differences in orbital periods, waiting for Earth's and Mars' orbits to be closely aligned can often be inefficient when planning a descent or ascent from Mars' surface. Rather, after the ascent from Mars, Venus can be used to gravitationally assist the spacecraft back to Earth. Since the spacecraft is much less massive than Venus, and they are orbiting in the same direction, counterclockwise, it can "steal" energy from Venus because Venus' energy loss will be negligible, but the spacecraft's energy gain will be substantial [17]. If the spacecraft passes behind Venus' direction of inertial motion, then it will gain energy and velocity (shown in Figure 14); however, if the spacecraft passes in front of Venus' direction of inertial motion, then it will lose energy and velocity because of a "gain of velocity" in the opposing direction.

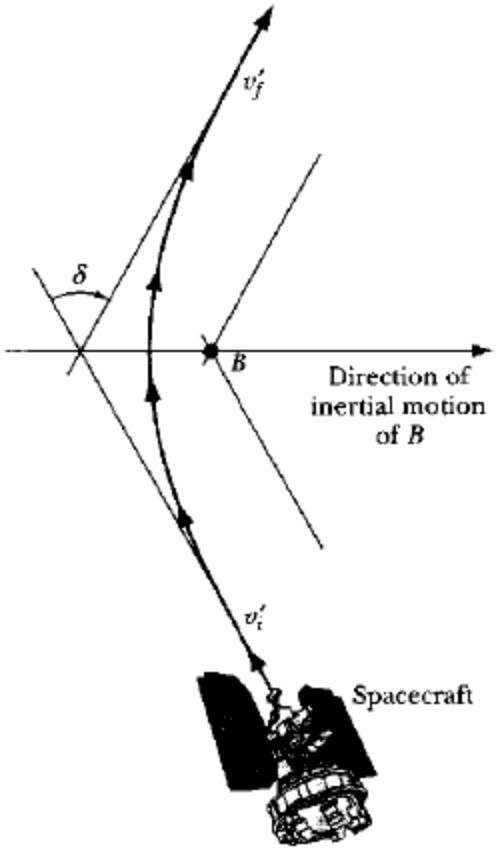


Figure 14: How gravity assist increases the velocity of a spacecraft passing behind a planet's direction of inertial motion [17]. In this context, the spacecraft is the incoming celestial object, B is a BH, and the direction of inertial motion points to the center of the orbit.

Although a substantial mass difference between two objects can improve gravity assist, this is not a requirement. For a star and a BH in the x-y plane with $M_* = M_{\mathrm{BH}}$ and equal and opposite velocities of $\vec{v}_{*,\mathrm{i}} = 100\frac{\mathrm{km}}{\mathrm{s}}$ and $\vec{v}_{\mathrm{BH,i}} = -100\frac{\mathrm{km}}{\mathrm{s}}$, the center of mass reference frame will have equal and opposite initial and final velocities represented by

$$\left(\vec{v}_{*,\mathrm{i}} - \vec{v}_{\mathrm{BH,i}}\right) = -\left(\vec{v}_{*,\mathrm{f}} - \vec{v}_{\mathrm{BH,f}}\right). \tag{2.5.13}$$

If the inertial reference frame is set to be at the star, then $\vec{v}_{*,\mathrm{i}} = 0\frac{\mathrm{km}}{\mathrm{s}}$ and $\vec{v}_{\mathrm{BH,i}} = -200\frac{\mathrm{km}}{\mathrm{s}}$; however, since inertial reference frames must stay at constant velocity, the observer will see $\vec{v}_{*,\mathrm{f}} = -200\frac{\mathrm{km}}{\mathrm{s}}$ and $\vec{v}_{\mathrm{BH,f}} = 0\frac{\mathrm{km}}{\mathrm{s}}$ [18]. Because of this, the star is boosted away from the BH due to the increase in velocity of the star and decrease in velocity of the BH, which is known as

gravity assist. In planetary travel, the planet will have less of a change in velocity, but the spacecraft will have more of a change in velocity in comparison to the equal mass star-BH case.

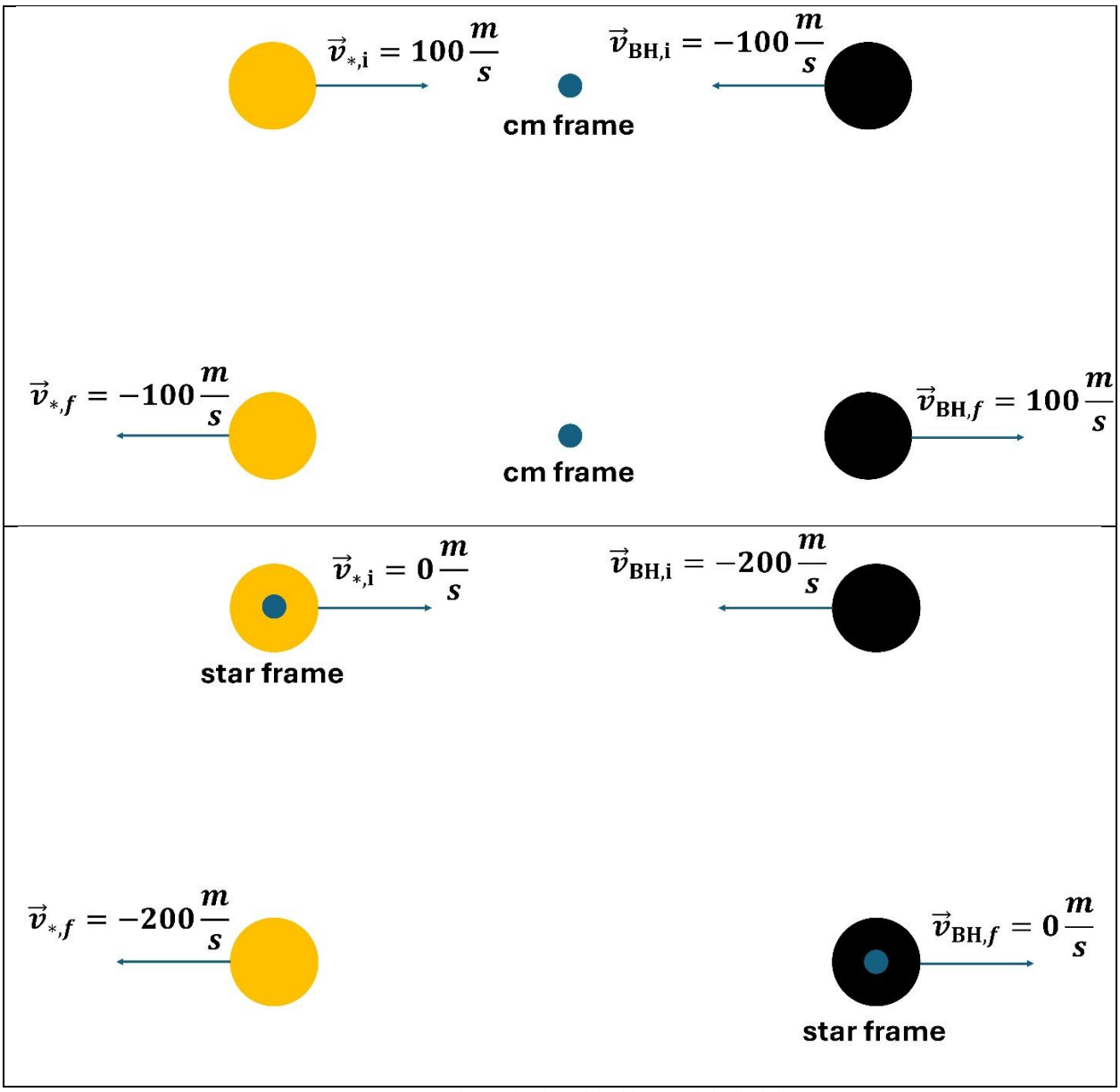


Figure 15: Gravity assist visualized by special relativity.
The yellow circle on the left is the star and the black circle on the right is the BH, but this also can happen with two BHs orbiting each other in a binary. The star and the BH are in a parabolic orbit that uses assumptions of a head-on elastic collision. The top frame shows this scenario with respect to the center of mass frame, which stays constant since there are equal mass objects moving at equal velocity. The bottom frame shows this scenario with respect to the star frame, which moves at a constant velocity, $\vec{v}_{*,\mathrm{i}}$, to the right, continuing even after the interaction. Each frame depicts before the interaction in the top portion and after the interaction in the bottom portion. The star's frame seems to have the star gaining lots of speed after the interaction, which shows a gravity assist of the star for this scenario.

2.5.6 Kick Velocity

As discussed in section 2.3.1, the escape velocity, v_{escape}, is the velocity needed for an

object to escape the gravitational pull of a celestial body. After an encounter between a BBH and a star, the BBH can receive a gravitational kick from the star either being destroyed or partially disrupted, giving it a kick velocity, v_{kick}. In a globular cluster, if v_{kick} is greater than the cluster's v_{escape}, then the BBH will leave the cluster, entering an area in space with little to no celestial objects to interact with. If this is the case, then we can assume $t_{\text{enc}} \to \infty$, meaning that large t_{GW} is no longer insignificant because there will be no subsequent encounters. For the cluster in this project (discussed more in section 3.1), the v_{kick} can be approximated to a range of $30 - 50\,\frac{\text{km}}{\text{s}}$, making an average $v_{\text{kick}} = 40\,\frac{\text{km}}{\text{s}}$ a safe choice. [19]. This is a useful phenomenon to consider when analyzing the merger outcomes of star-BBH interactions.

3. Methodology

To study these star-BBH collisions, I will be examining results from many different codes: *Cluster Monte Carlo*, *Modules for Experiments in Stellar Astrophysics*, a Python three-body integrator, and *StarSmasher*. This methodology, shown in Figure 16, has been in progress since first collecting data in the summer of 2023.

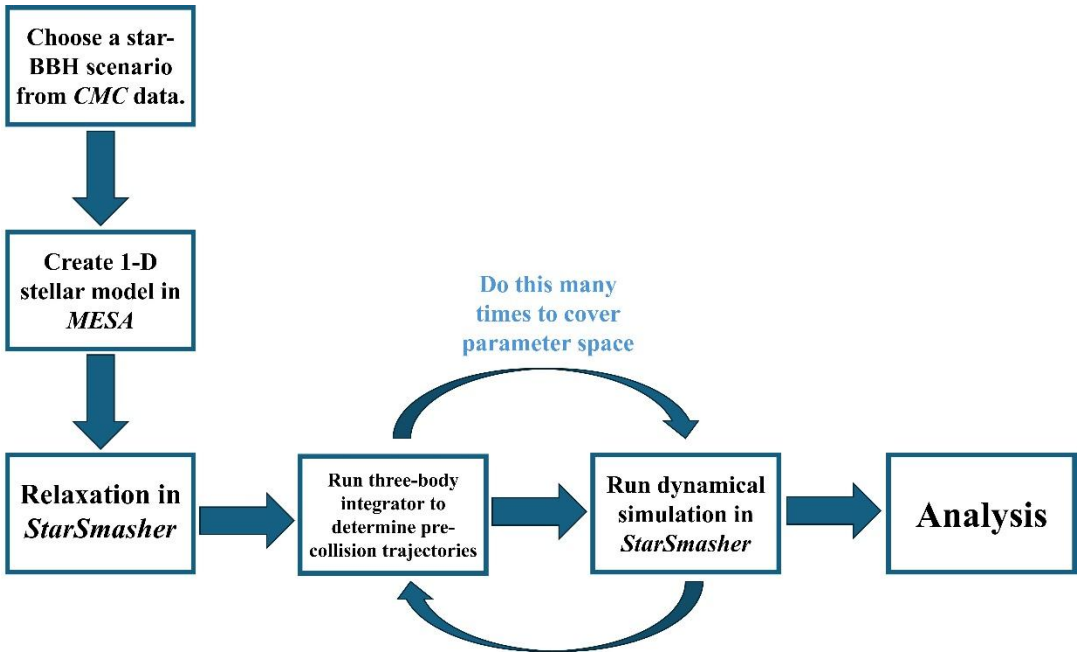


Figure 16: The methodology of this research.
Step 2 is 1-dimensional, and steps 3, 4, and 5 are 3-dimensional codes.

3.1 Cluster Monte Carlo Code

Cluster Monte Carlo (CMC) is an *N*-body code for collisional stellar dynamics [20]. *CMC* represents a system of *N* particles interacting with one another via the gravitational force and portrays how the system will evolve over time. The Monte Carlo method uses repeated random sampling to obtain numerical results [21]. *CMC* is often used to find the most probable astrophysical interactions for a given scenario. Before running a more computationally costly SPH simulation, it can be efficient to search for the most common scenarios by surveying the parameter space so that you are able to motivate your research. See Table 1 for initial values for the scenarios chosen from *CMC* to run in *StarSmasher*. The cluster I am studying has $N = 8 * 10^5$ stars, $Z = [0.1, 1]\ Z_\odot$ (with $Z_\odot \approx 0.0187$ [22]), an initial virial radius $r_\mathrm{v} = [0.5, 1.0]$ pc, and a primordial binary fraction for massive stars $f(> 15\ M_\odot) = 100\%$, meaning all stars greater than this mass value are in a binary at the start of the simulation. The older age of the cluster I am studying motivates the metallicity value for my star in section 3.2, $Z = 0.002$, as explained in section 2.2.3.

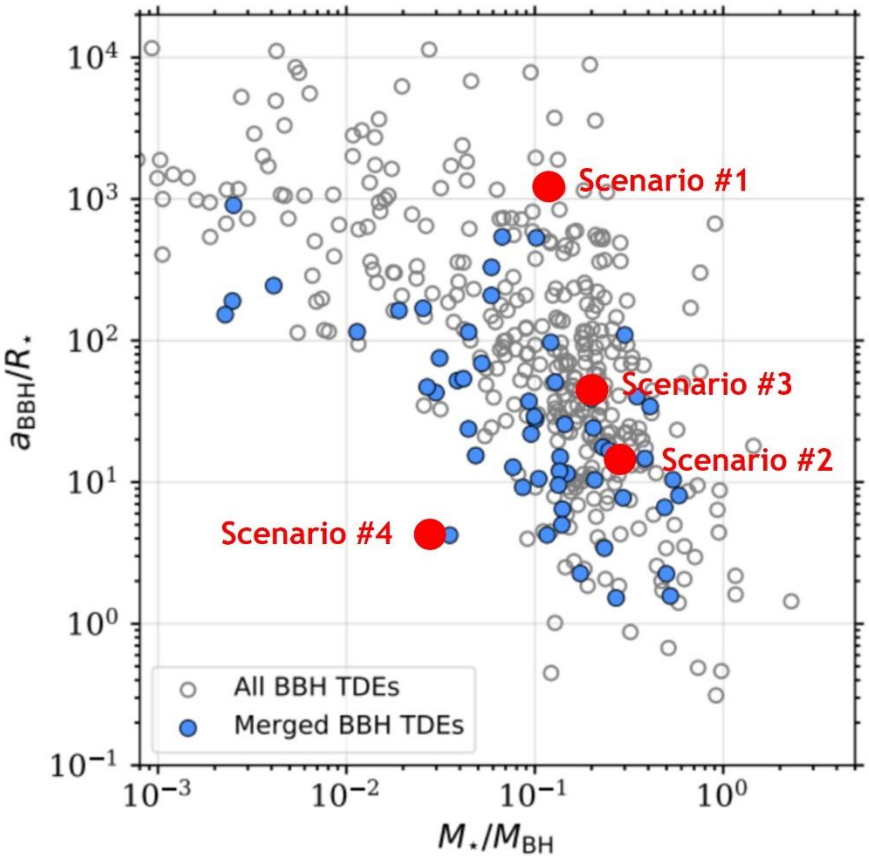


Figure 17: Northwestern *CMC* data with Allegheny SPH scenarios overlaid [3].
During the summer of 2023, myself, Emma Chambers, and Dr. James C. Lombardi, Jr. chose separate scenarios of a pre-MS or MS star interacting with a BBH (scenarios #1, #2, and #3) based on their proximity in parameter space to other scenarios from *CMC* data. I also chose an RG-BBH scenario to study (scenario #4). For each of these scenarios, a variety of SPH simulations were run with different orbital orientations (explained in Sections 2.5.1 and 3.3). The y-axis is the normalized initial semi-major axis of the BBH (with respect to the initial radius of the star, which does not get altered from collisions in N-body simulations) and the x-axis is the normalized stellar mass (with respect to the mass of the BH causing disruption) [3]. Blue dots represent TDEs that result in a BBH merger after the stellar interaction, and white dots represent non-merger scenarios.

Scenario	Type	M_* ($M_\odot$)	R_* ($R_\odot$)	M_{BH1} ($M_\odot$)	M_{BH2} ($M_\odot$)	a_{BBH} ($R_\odot$)	e_{BBH}	v_∞ ($\frac{km}{s}$)
#1	MS	1.00006	1.04151	7.48560	7.52296	1204.43	0.389	5.03668
#2	MS	9.59834	8.14164	29.1534	27.8599	122.029	0.913	16.5455
#3	MS	10.1108	7.19253	36.5594	39.5646	338.372	0.417	75.7795
#4	RG	3.95943	31.4825	130.477	102.868	97.7074	0.308	47.0738

Table 1: Initial values for the chosen *CMC* scenarios (before collision).
Type indicates main sequence (MS) or red giant (RG) and v_∞ is the velocity at infinity, meaning the theoretical velocity of the star at infinite distance away from the BBH.

3.2 Modules for Experiments in Stellar Astrophysics Code

Our knowledge of the physical and chemical properties of stars allows us to simulate

evolutionary sequences to generate the exact quantities necessary to create an SPH model of a star (discussed in Section 3.4.2) that we want. *Modules for Experiments in Stellar Astrophysics* (*MESA*) is a one-dimensional stellar evolution code that, from an inputted mass (M_*) and metallicity (Z), can evolve a star over time, allowing the user to choose a data file from a specific time in its evolution to gain information about the star [23]. Although some important aspects of a star are three-dimensional (e.g. convection, rotation, and magnetism), accurate one-dimensional simulations give useful information for the creation of three-dimensional models in codes such as *StarSmasher* [24]. *MESA* outputs data into human-readable `profile.data` files for every timestep. These files can be interpreted using Python to plot an H-R diagram for the star. An H-R diagram for scenario #2 and #3's *MESA* models for the stars from Figure 17 are shown in Figure 18. Both models used $z = 0.002$, consistent with stars present in distant globular clusters [25].

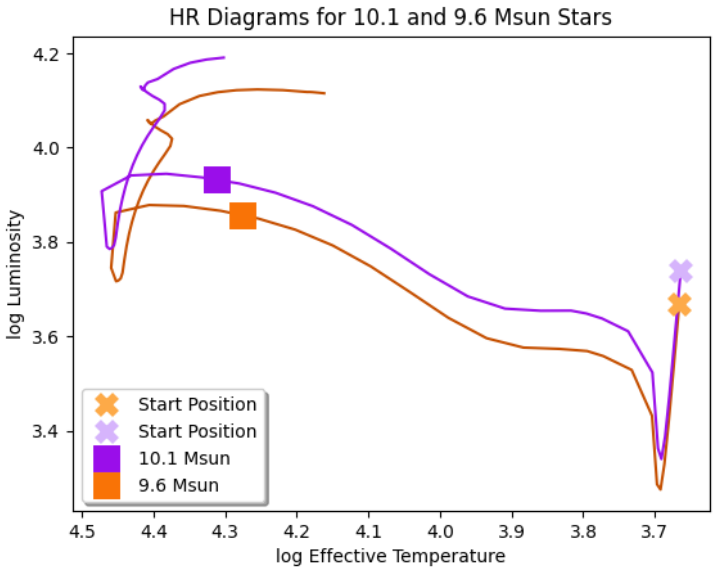


Figure 18: An H-R diagram for scenario #2 and #3's *MESA* model stars later used for SPH calculations in *StarSmasher*. The square points are the locations of the `profile.data` files that were chosen for further use in creating *StarSmasher* models of the stars, and their locations show that they are both on the MS, motivated by Figure 2.

3.3 Pre-Collision Trajectory Three-Body Integrator Code

Before working with *StarSmasher*, since I am looking at the effects of the orbital parameters discussed in Section 2.5.1 on final χ_{eff} values, it is useful to provide myself with an approximation of which orientations of the BBH will lead to a collision with the star and which

will not. Since some orientations will not lead to a collision, I do not want to waste SPH computation time on cases that are trivial. Dr. Lombardi developed a three-body integrator Python code that acts like *CMC* in the way that it computes gravitational interactions between three particles at differing initial orientations. It is unlike *CMC* in that it does not use random sampling of *N* particles and rather takes evenly stepped intervals of BBH angles (ω, i, Ω, ν) that are provided by the user to simulate the three-body star-BBH interaction. A file is output that provides these angles, if a collision occurred, and if so, then initial position and velocity vectors are printed which can be given as input to *StarSmasher*. The code decides that a collision occurs if the star approaches one of the BHs within 2 r_t, and if so, takes position and velocity values from when the star was 10 r_t away to give to *StarSmasher*. One can then imagine compiling all the collision cases and randomly picking some to run dynamically in *StarSmasher*. See Figure 19 for a visual representation of an example three-body integration that led to a collision. More information on this code can be found in **Appendix A**.

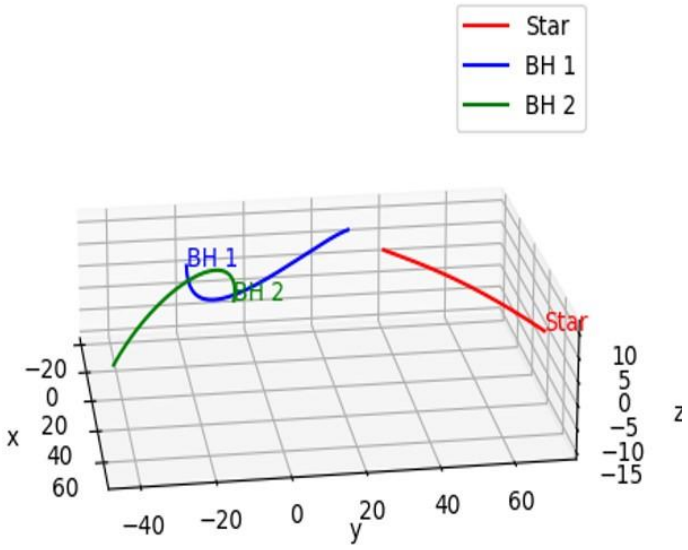


Figure 19: An example of three-body integration of a collision case for scenario #2.
The labels represent the beginning of the integration, with the opposite end of the lines being the end of the integration. As shown, the star approaches within a close distance of BH1 (2 r_t), therefore there will be a collision for this set of angles ($\omega = -36°, i = 120°, \Omega = 180°, \nu = 108°$) [26].

3.4 *StarSmasher* Code

We simulate stellar model relaxations and dynamical collisions using *StarSmasher* [6]. A *MESA* profile can be used as input to relax a three-dimensional model in SPH. With a relaxed stellar model, this can collide with another star, a point-mass BH, or even a planet.

3.4.1 Smoothed-Particle Hydrodynamics

A popular method of simulation is mesh-based, where each element (cell) has physical quantities associated with it, and the mesh can either be static (Eulerian), adaptive (Lagrangian), or a combination. With high energy physical scenarios, this may cause material to move through the mesh at very high speeds, causing an Eulerian mesh to make very small time steps, or a Lagrangian mesh to tangle: high material speeds cause the mesh to have a change in volume greater than the volume that is available, $dV > V$, creating negative volume elements. To fix these problems, smoothed-particle hydrodynamics (SPH) can be used where each element is represented as a node (particle), with N number of particles interacting as a fluid with one another. Each particle has an analytical weighting function (kernel) to determine how much of an effect nearby particles (neighbors) will have on it. With a particle having a smoothing length, h, the kernel is supported by a value of $2h$. This method is Lagrangian but removes the problem of mesh tangling since there is no mesh; however, particles bunching together (often near BHs due to their strong gravitational influence) can cause small time steps and small smoothing lengths. To fix this, particles can be eroded, deleting their existence and physical quantities from the problem, simulating the BH eating the mass. Although this will cause less energy conservation, it is an efficiency-accuracy tradeoff that is useful for problems involving complex dynamics.

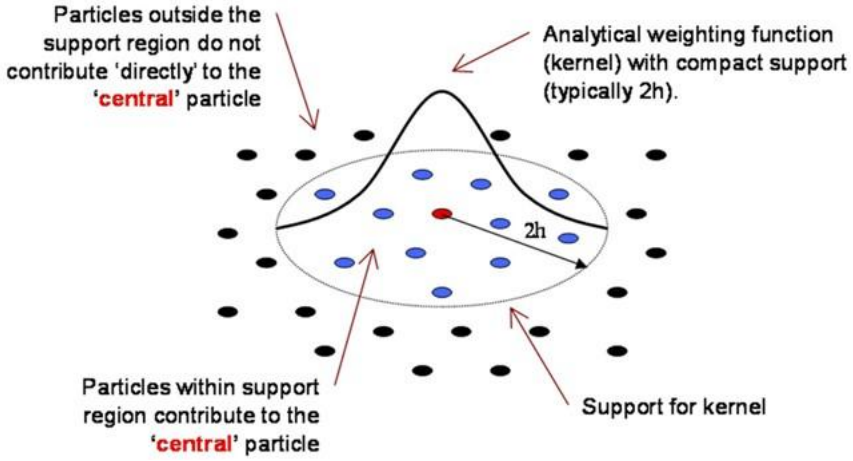


Figure 20: Visual representation of an SPH Wendland C4 kernel.
The blue particles are neighbors to the central particle because they are within a radius of $2h$ of the central particle [27].

The kernel mentioned above is a density weighting function that is used for each particle in a simulation. As shown in Figure 20, the neighbors closest to the central particle count more

towards the central particle's density. With neighbors i and central particle j, this density is represented as

$$\rho_{\mathrm{j}} = \sum m_{\mathrm{i}} W_{\mathrm{ij}} \tag{3.4.1}$$

where W_{ij} is the kernel weighting function. *StarSmasher* uses a Wendland C4 kernel. Along with density, velocity and internal energy derivatives can be calculated, as shown in appendix A of Gaburov et al. [6].

3.4.2 Relaxations

The importance of relaxation is to create a three-dimensional model of a star from the one-dimensional *MESA* model. When the *MESA* model is first transferred to *StarSmasher*, there is an abundance of energy given to the particles, causing the star to not be in hydrostatic equilibrium (see Figure 21). Some of this energy needs to be released, therefore relaxing the star. SPH particles are initially laid in a hexagonal rigid lattice, and throughout a good relaxation, a more spherical star is seen to be formed. There are a few different plots to keep track of during a relaxation to tell if it is running correctly or not, and there are input parameters that directly change how these plots will look (see Figure 23).

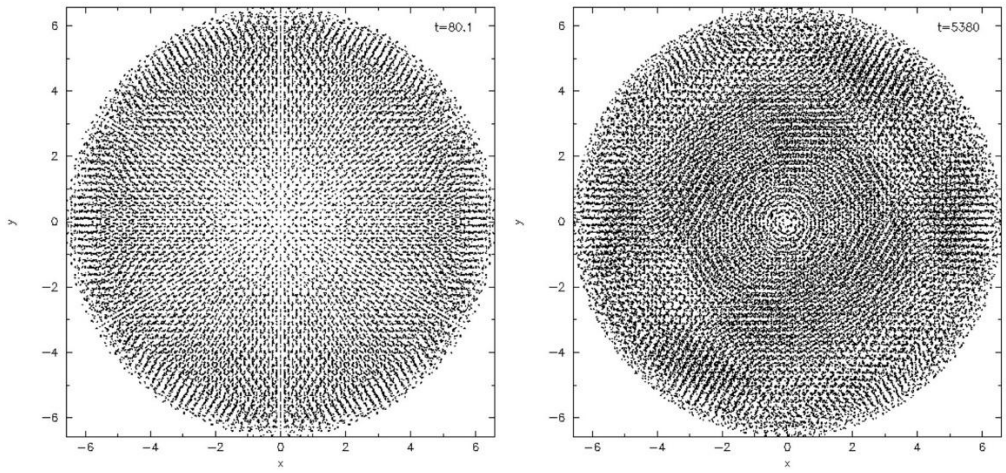


Figure 21: 9.6 $M_{\odot}$ MS star (scenario #2) relaxation, visualized using *SPLASH* [28].

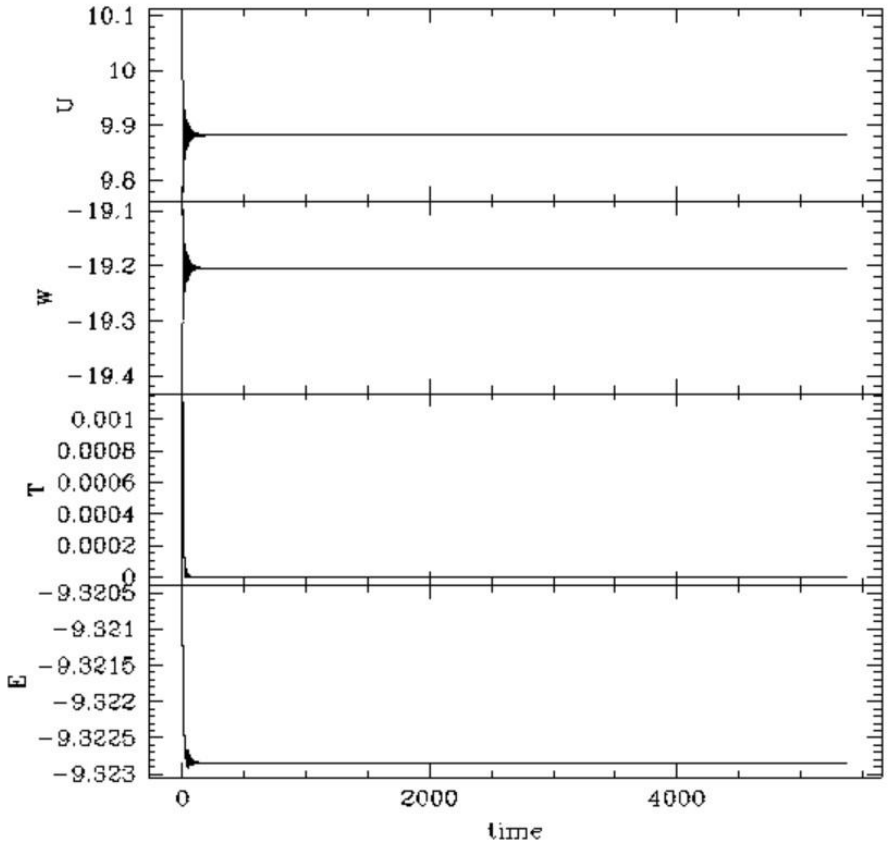


Figure 22: Energy vs. time plots for scenario #2's star SPH relaxation.
The plots help exemplify the initial abundance of energy from the *MESA*-to-*StarSmasher* transition, and how this eventually levels out. Because of this energy abundance, *StarSmasher* particles are initially moving around. An artificial drag force is applied to slow down the particles until they stop moving, which is the reason for the initial oscillations in the energy plots. Eventually, the total energy levels out to a constant value, resulting in a successful SPH relaxation. The plots from top to bottom are: Internal energy, gravitational potential energy, kinetic energy, and total energy, all in code units of $\left[\frac{GM_\odot^2}{R_\odot}\right]$.

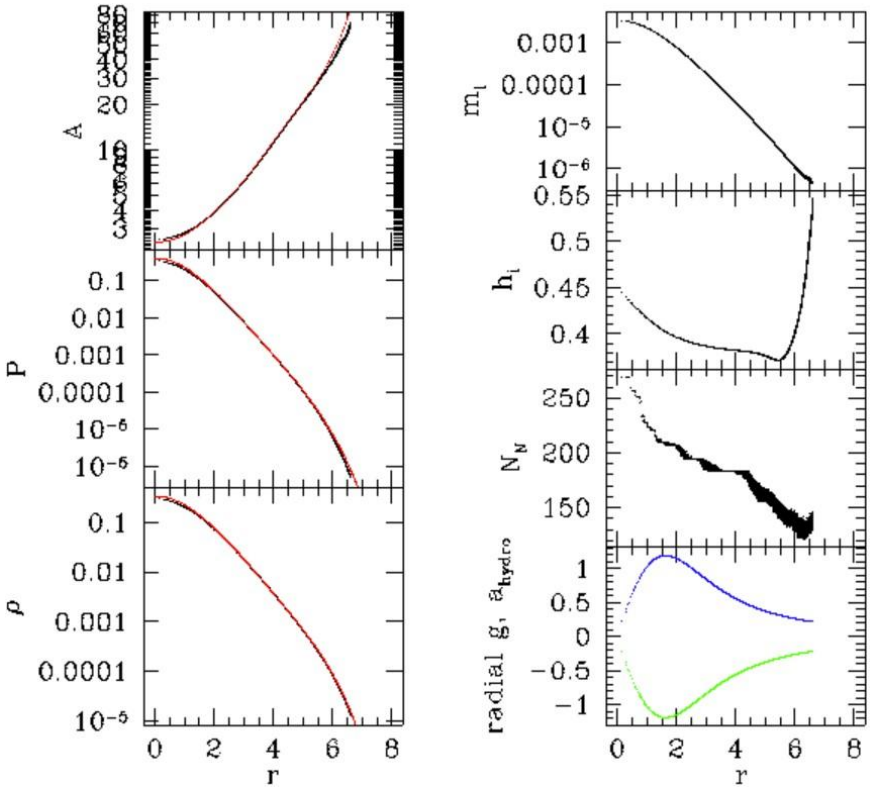


Figure 23: Various values vs. radius of the relaxing scenario #2 star.
$A = P/\rho^{\frac{5}{3}}$, P is pressure, ρ is density, m_i is the mass of each particle, h_i is the smoothing length of each particle, N_N is the neighbor number of each particle, and the lower right plot shows hydrostatic equilibrium between the gravitational acceleration (green) and hydrodynamic acceleration (blue) for each particle.

In each of the plots in the left column of Figure 23, there is a red line and black dots. The red line is some mathematical function that we want the black dots (SPH particles) to line up with. Because of this logic, I concluded that the SPH particles have reasonable pressure and density for this model.

The plot of N_N vs. r is the neighbor number for each particle. It is good to note that the minimum neighbor number for a particle is no less than ~130, which proves there is enough resolution to create valid results. We want about 150 neighbors at early times of the relaxation, and to do that we use Equation 3.4.2 with values h_floor of 0.15, h_ceiling of 10,000, and b on the scale of 100

$$h_\mathrm{i} = \left(\frac{1}{h_\mathrm{ceiling} - h_\mathrm{floor}} + b\rho_i^{\frac{1}{3}}\right)^{-1} + h_\mathrm{floor}, \tag{3.4.2}$$

where ρ_i is the density of particle i, to determine the smoothing length of particle i, and therefore its number of neighbors [29].

To alter a relaxation, several parameters in *StarSmasher*'s input file can be changed. For example, *NNOPT* controls the maximum neighbor number, h_{floor} sets a minimum smoothing length, h_{ceiling} sets a maximum smoothing length, *EQUALMASS* sets if particles have equal mass (*EQUALMASS*=1) or constant number density (*EQUALMASS*=0), and T_{relax} is the time scale necessary to calculate the artificial drag acceleration on particle *i*, $\vec{a}_{\mathrm{i,drag}} = -\vec{v}_{\mathrm{i}} / T_{\mathrm{relax}}$. An artificial drag force is used to keep the initial abundance of energy from expanding the star out to a large radius and disrupting the integrity of the star, discussed in Figure 22. Eventually this drag force is turned off depending on the value of T_{reloff}.

3.4.3 Dynamical Collisions

Another function of *StarSmasher* is used to collide the star with the BBH. The particles are treated as fluid-like blobs to accurately simulate collisions. We chose an arbitrarily even amount of coplanar and off axis cases to study when choosing which three-body integration results to use. When a case is decided, the position and velocity vectors output from the three-body integrator can be copied into a file arbitrarily named `input.3s`, which is set as an input file for *StarSmasher* in `sph.input`.

Since we cannot create realistic models of BHs, they are treated as singular SPH particles with zero spin, for simplicity. Since the BHs start with zero spin, we can tell how much of an effect that mass transfer had on altering the spin of the BH and angular momentum of the accretion disk. This provides us with valuable information on how the spin of these systems evolve with respect to mass transfer.

3.5 Post-Processing Analysis

StarSmasher outputs data in binary files which means they are not human readable. To pull the data from these files, a Fortran post-processing code is used, which reads the binary files, and does whatever analysis we code it to do. Depending on the dynamics of the simulation (star-BBH collision, star-star collision, star-BH collision, etc.), different post-processing code must be used. I have been working with a Fortran code named "splotBBH", originally created by Dr. Lombardi, but altered throughout time by Emma Chambers and myself. The routine in this code I use is the creation of a `massAndMore.out` file, which includes physical properties of the dynamical *StarSmasher* simulation. The values calculated and printed to this file can be changed

by altering the Fortran code. For every simulation time step, a value (e.g. mass of BH1) is calculated and saved to `massAndMore.out`, allowing me to gather physical quantities for every step of the simulation to use for further analysis. This is often useful to see how a value changes over the time of the simulation, or with respect to another value.

4. Results and Analysis

For this project, I simulated twenty-two dynamical interactions for scenario #2, varying initial input for the four rotational degrees of freedom: i, ν, ω, and Ω. There were three types of final outcomes: total tidal disruption (TDE), delayed tidal disruption (DTDE), and partial disruption with stellar ejection (PTDE). A TDE consists of the star being destroyed from the first interaction with the BBH, a DTDE consists of the star being partially disrupted on its first interaction with the BBH but, within a time less than t_{enc}, becoming destroyed after one or more subsequent interactions, and a PTDE consists of the star being partially disrupted by the BBH one or more times and eventually being ejected from the BBH system.

Due to differences between initial orbital configurations, the outcomes varied heavily from case to case. Therefore, a global stopping condition was not used. Instead, I chose when to stop each simulation based on a few criteria: whether the BBH is in a tight orbit; for stellar ejection, how much time has passed since the star has been ejected; and whether stellar ejection and mass transfer have stopped or are, for the most part, negligible.

Case #	Orbital Parameters	Outcome	$\chi_{\mathrm{eff,f}}$	$t_{\mathrm{GW,i}}$ (Myr)	$t_{\mathrm{GW,f}}$ (Myr)	$v_{\mathrm{kick,f}}$ (km/s)
1	i000_a-108_p-036_l036	TDE	0.0696	8,231.01	30,734	9.691
2	i000_a108_p-108_l-108	TDE	0.1907	5,058.57	4,204.5	41.84
3	i000_a108_p180_l180	TDE*	0.0913	4,367.08	DNE	DNE
4	i041_a-108_p108_l036	TDE	0.0807	5,296.36	7,699.8	23.64
5	i041_a-108_p-108_l108	DTDE	0.0448	4,468.59	11,215	14.42
6	i060_a036_p108_l036	PTDE	0.0055	2,923.78	11,134	35.44
7	i060_a108_p108_l036	PTDE	0.0020	2,769.88	13,353	52.36
8	i060_a180_p108_l-036	PTDE	0.0034	389.79	445.29	1.734

9	i076_a-036_p-036_l180	PTDE	0.0050	1,775.42	2,893.1	40.34
10	i076_a180_p108_l-036	PTDE	0.0083	676.79	1,347.5	18.93
11	i104_a-036_p-036_l180	DTDE	0.0229	1,162.66	493.84	5.563
12	i104_a108_p-036_l180	PTDE	0.0064	1,211.77	539.42	18.76
13	i104_a-108_p108_l036	PTDE	0.0014	1,576.19	4,766.4	53.06
14	i120_a-036_p-036_l180	TDE	0.0381	1,070.55	71.820	19.21
15	i120_a036_p-036_l180	TDE	0.0360	1,081.75	62.810	19.71
16	i120_a108_p-036_l180	DTDE	0.0268	1,132.99	93.360	10.69
17	i120_a-108_p180_l036	PTDE	0.0004	2,025.76	0.1700	73.80
18	i120_a180_p108_l-036	DTDE	0.0402	2,233.17	101.51	18.36
19	i139_a-108_p-036_l180	DTDE	0.0081	1,242.03	107.35	15.41
20	i139_a180_p-036_l-108	DTDE	0.0549	2,215.50	774.75	13.81
21	i180_a-036_p-036_l-036	TDE	0.0000**	70.49319	0.00041	72.44
22	i180_a180_p108_l036	PTDE	0.0008	4,357.74	16.500	32.13

Table 2: All 22 simulations for scenario #2: the 9.6 $M_\odot$ pre-MS star interacting with the 57.0 $M_\odot$ BBH. Rather than the Greek lettering used for the orbital parameters discussed in Section 2.5.1, the case labels here use i for inclination, a for true anomaly, p for argument of periapsis, and l for longitude of the ascending node. Cases are ordered by increasing inclination angle, i. Outcomes are shaded by type for visual purposes: green for TDEs, blue for delayed TDEs with stellar destruction, and orange for partial TDEs with stellar ejection. Case #3 has an * to denote the final state as an unbound, hyperbolic BBH ($e_{\mathrm{BBH,f}} > 1$), meaning that the BBH will not inspiral; therefore, this case will be disregarded for the following analysis. The highlighted χ_{eff} are cases that have a change from negative to positive χ_{eff} at any point in the simulation, suggesting a spin flip. Case #21 has a ** to denote a final $\chi_{\mathrm{eff}} = 0$, which is due to SPH mass ejection, discussed further in Figure 25.

Case #	$L_{\mathrm{BBH,f}}$ $[\mathrm{GM}_\odot^3\mathrm{R}_\odot]$	$a_{\mathrm{BBH,f}}$ $(\mathrm{R}_\odot)$	$e_{\mathrm{BBH,f}}$	$L_{\mathrm{BBH-Star,f}}$ $[\mathrm{GM}_\odot^3\mathrm{R}_\odot]$
1	701.70	385.638	0.946477	0.00
2	679.34	43.6162	0.460235	0.00
3	805.48	-466.749	1.05253	0.00
4	695.32	48.5882	0.442976	0.00
5	650.63	153.594	0.877523	0.00
6	697.26	55.4332	0.495421	943.85
7	711.32	58.9918	0.510159	422.11
8	412.54	94.184	0.918834	6,351.62
9	572.30	56.7655	0.709477	705.06
10	504.49	66.9118	0.820748	1,004.09
11	460.60	39.1424	0.735285	0.00
12	448.03	55.2091	0.829264	316.17
13	613.29	58.132	0.664423	2,162.67
14	353.75	33.5088	0.828886	0.00
15	347.15	33.0508	0.833336	0.00
16	363.97	35.0951	0.825033	0.00

17	139.88	37.7206	0.977344	591.17
18	369.45	36.9312	0.831194	0.00
19	285.31	662.624	0.994821	0.00
20	449.32	121.651	0.928915	0.00
21	73.24	2.62153	0.90724	0.00
22	253.31	90.5054	0.9689	148.53

Table 3: A continuation of Table 2, but with physical data.
For the same explanation as Table 2, case #3 is highlighted, and the reasoning can be seen by the $e_{\mathrm{BBH,f}} > 1$.

A few cases provide irregularities to the data set. Case #3 has a $e_{\mathrm{BBH,f}} > 1$ after the interaction with the star, meaning the BBH will not merge. Because of this, I have removed the data regarding this case from any relevant analyses going forward. Also, due to a remarkable coincidence in how the star and BBH line up, the collision in Case #21 causes the orbit of the BBH to come to a halt, leading to a very tight binary immediately after the star is destroyed. Because of how close the SPH particles get to one another near the BH, the particles are ejected off the BH. The timescale of this process is within a few hundred code time units, shown in Figure 25, with this unit relating to time as

$$1\ t_{\mathrm{code}} = \sqrt{\frac{R_{\odot}^{3}}{G M_{\odot}}} \approx 26.54 \text{ minutes.} \tag{4.1}$$

The speed of this inspiral and the ensuing mass ejection causes $\chi_{\mathrm{eff,f}}$ to be reported as zero, but it should be noted that the spin was flipped from negative to positive before this, as shown in Figure 25. This phenomenon is expected to be caused by the tight alignment between the BHs and the star, likely an outcome of the geometrical parameter space chosen.

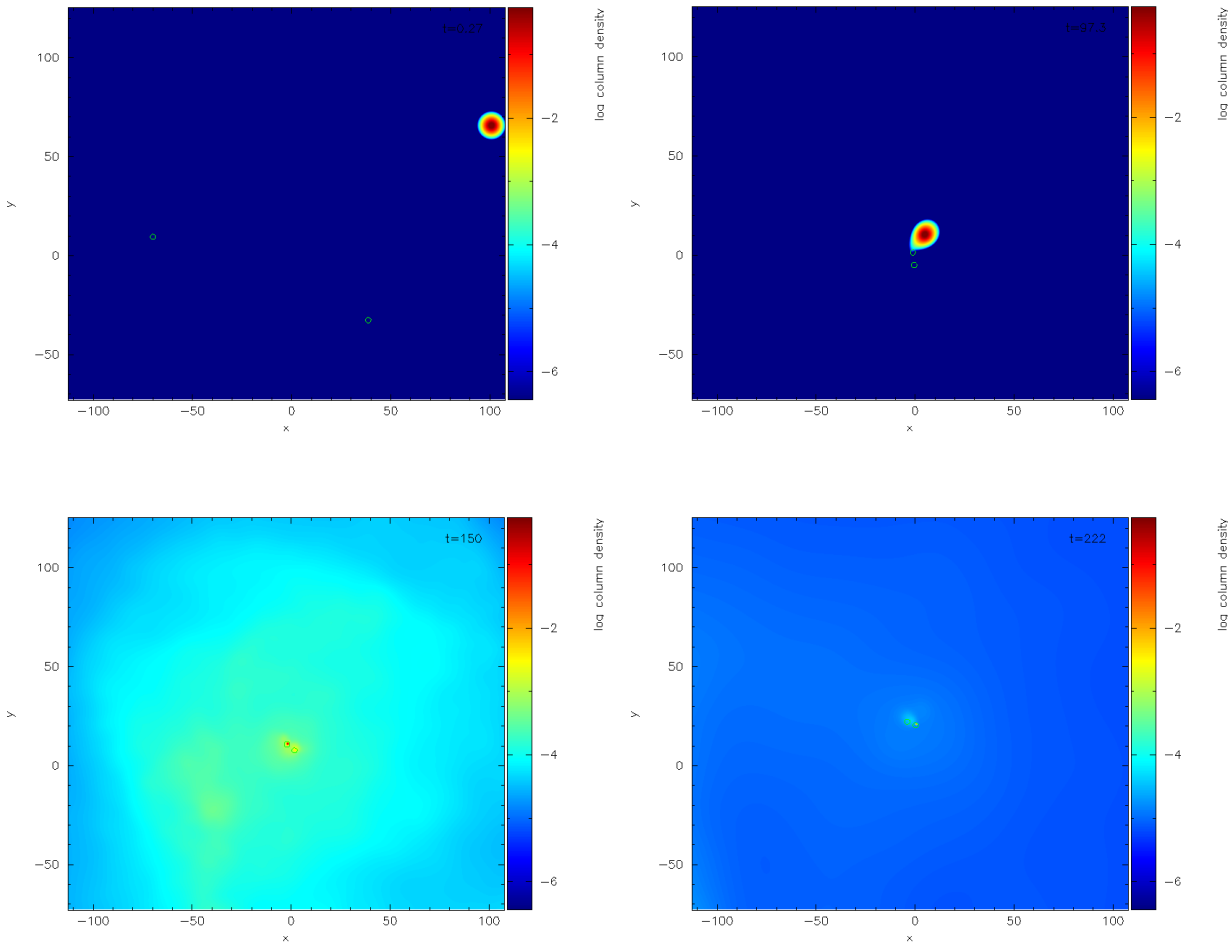


Figure 24: Visualization of Case #21 in *SPLASH* as a column density, which is 3-dimensional density projected onto the 2-dimensional x-y plane [28].

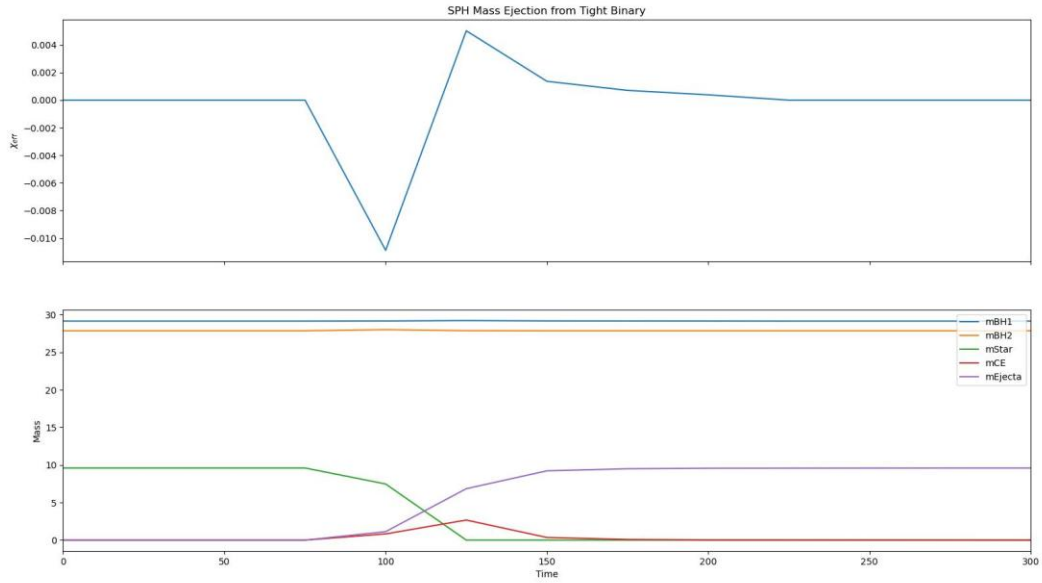


Figure 25: Case #21's mass ejection from SPH due to a fast-forming tight binary.
Although χ_{eff} does vary during the collision process, it levels out at a value of zero because all the star's mass is transferred to ejected mass. Due to how fast this process is, I have reported $\chi_{\text{eff,f}} = 0$; however, it should be noted that no other case discussed was ran to this state. MBH1 and MBH2 are the masses of BH1 and BH2, MSTAR is the mass of the star, MCE is the mass of the common envelope of stellar mass around both BHs, and MEJECTA is the mass ejected from the system.

Before continuing, the code's validity can be expressed by plotting various angular momenta and spins as well as the total angular momentum to show that this total is constant, therefore proving conservation. Figure 26 expresses these values for case #2, which is a coplanar TDE; however, this can analogously be plotted for any non-coplanar case. Conservation of angular momentum is necessary, and this plot helps exemplify different aspects of angular momentum transfer such as between LBBHz and Lstaroriginz during the stellar destruction.

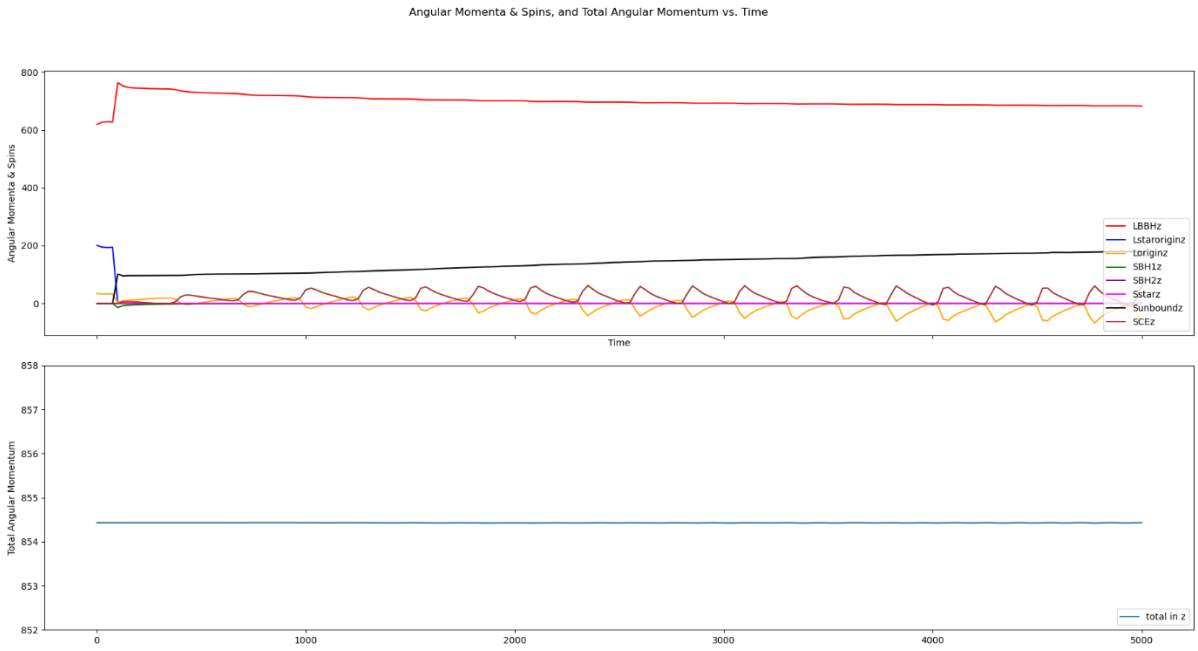


Figure 26: Various angular momenta and spins plotted together along with the total angular momentum of the system vs. time in code units.
LBBH is the angular momentum of the BBH, *Lstarorigin* is the angular momentum of the star with respect to the origin, *Lorigin* is the angular momentum of the BBH with respect to the origin, and *SBH1, SBH2, Sstar, Sunbound,* and *SCE* are the spin angular momenta of BH1, BH2, the star, the unbound mass, and the common envelope respectively. The origin is defined as the center of mass for the entire system. Note that $L_{\mathrm{BBH,star}}$ is not listed here; however, it is still a useful quantity to discuss. All values are in the z-direction due to the coplanar nature of this case.

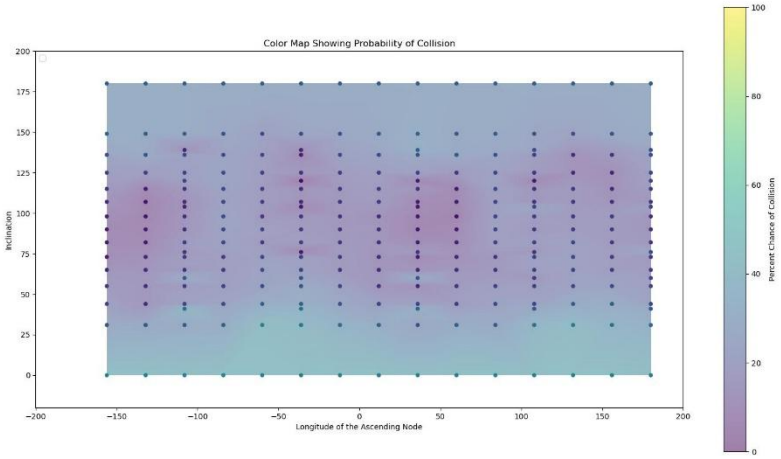
4.1 Collision Probabilities

To following color map plot shown in Figure 27 motivates the randomness of the cases chosen to run in *StarSmasher*. Since I chose three-body integrator cases arbitrarily, I hope to prove that my assortment of cases is effectively random and is sufficient to eliminate any biases. This plot is for scenario #2, but similar plots can be made for all other scenarios.

Looping through all cases from the three-body integrator output, the inclination (i) is plotted against the longitude of the ascending node (Ω). For each of these points, the other two angles, argument of periapsis (ω) and true anomaly (ν), are looped through, and a probability of collision is found by calculating the ratio of cases found to cause a collision to the total cases, $P =$ # of collisions / # of total cases, with the total case being on the order of less than ten. This probability is represented by color. Rather than plotting the colored points, I used a linear interpolation to create a color gradient.

I chose to plot i vs. Ω because this combination showed the widest range of angles. The only angle that is worse to focus on is ν. Because of its nature as the phase of the BBH orbit, it is time dependent, meaning the initial distance we start the star from the BBH in the simulation will alter this value, making it less of an intrinsic property of the BBH and more of a value that varies with time, as discussed in Section 2.5.1.

The cases I chose to run in *StarSmasher* are represented by dotted circles in the second plot of Figure 27. The values of ω and ν are further visually represented by vectors spanning values from $-180°$ to $180°$, with an angle of $0°$ represented by a vector pointing to the right, parallel to the x-axis, an angle of $90°$ pointing up, parallel to the y-axis, etc.



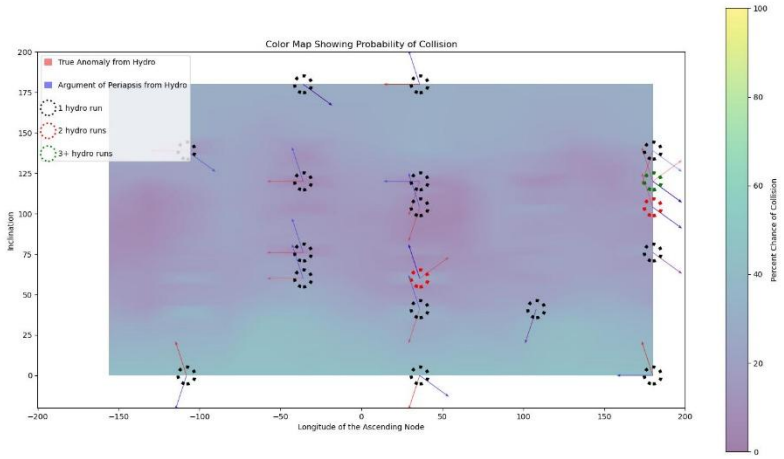


Figure 27: Probability plot for scenario #2.
The top plot shows the three-body integrator data used to make the color gradient. The bottom plot shows the cases chosen to run in *StarSmasher* ("Hydro"), represented by dotted circles, with varying colors containing the information that ν and ω can be varied at constant i and Ω, giving the possibility of running multiple dynamical simulations. The plot shows i vs. Ω, with ω and ν represented by arrows. Some arrows are overlaid on top of each other for the same "Hydro" point, shown by darker lines, which is the result of the ν and/or ω staying constant between cases or changing to a value from a different "Hydro" point.

As shown in Figure 27, the *StarSmasher* cases seem to be well spread out, motivating the randomness of my choices. The areas of highest probability are near $i = 0°$ and $i = 180°$, which are coplanar, parallel and anti-parallel, cases, as shown in Figure 11. This makes sense because if the star and BBH are in the same plane, the degree of freedom for the z axis is removed, making their collision probability the highest.

4.2 Positive χ_{eff} Convergence

By using the calculations described in Section 2.4.2, the χ_{eff} parameter can be plotted vs. time to monitor how well it averages out to small but positive values, motivated by the data discussed in Figure 1. Figure 28 proves that the data for scenario #2 converges to positive χ_{eff} values, which supports the data discussed in section 1.2. Not all simulations were run to the same time due to their dynamic differences, as discussed in the beginning of section 4.

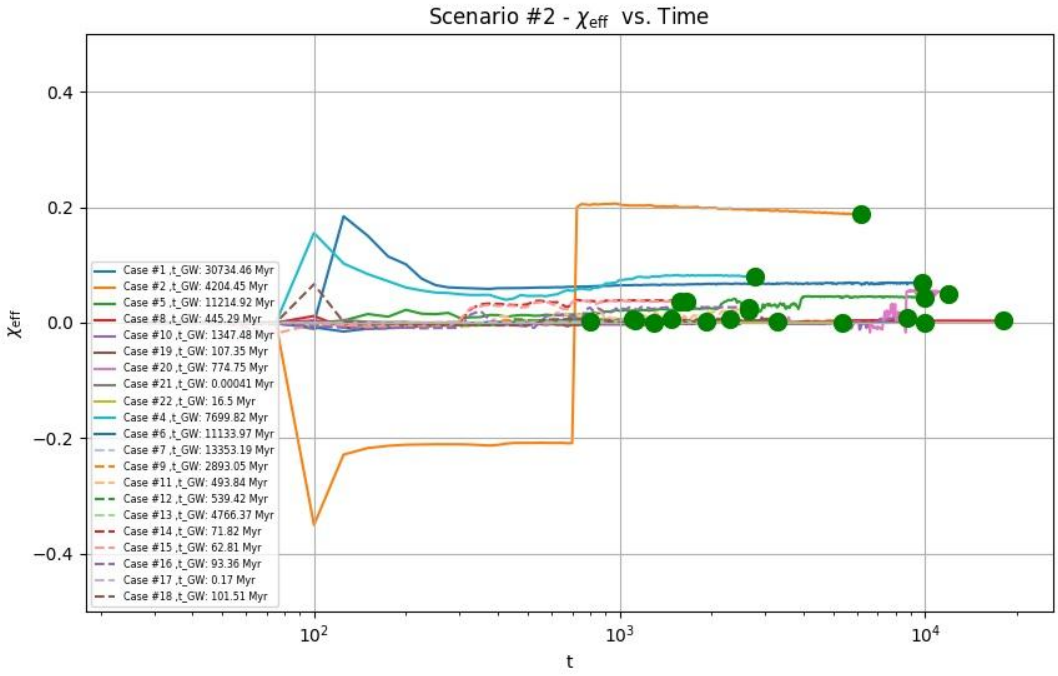


Figure 28: χ_{eff} vs. $time$ for all scenario #2 *StarSmasher* simulations.
Green dots denote final $\chi_{\text{eff}} \geq 0$, showing that all cases end with positive χ_{eff}. As shown, most cases end with small but positive χ_{eff} values. The BBH merger timescale, t_{GW}, is shown next to the labels for each case. Case #3 is not shown here.

4.3 χ_{eff} Flip Criteria and Outcomes for Coplanar Cases

The simplest case to study is coplanar, where all bodies are in the same plane, which includes the $i = 0°$ and $i = 180°$ cases. To discuss the criteria for a spin flip, analyzing these simpler cases will assist with making conclusions since the problem is now in two dimensions rather than three dimensions. This will help reduce errors in judgment and in reporting relationships between variables.

Cases #1 and #2 are both coplanar but one induces a flip in χ_{eff} from negative to positive and the other does not. A flip occurs when the accretion disk is initially spinning in the opposite direction of the orbit of the BBH, and then the BBH torques the disk to eventually spin in the same direction as the orbit, which can be seen by equation 2.4.1. Case #1 does not involve a spin flip because of the star's incoming trajectory being over the top side of BH1; however, case #2 does involve a spin flip because of the star's incoming trajectory being through the underside of BH1, as explained in section 2.5.5.

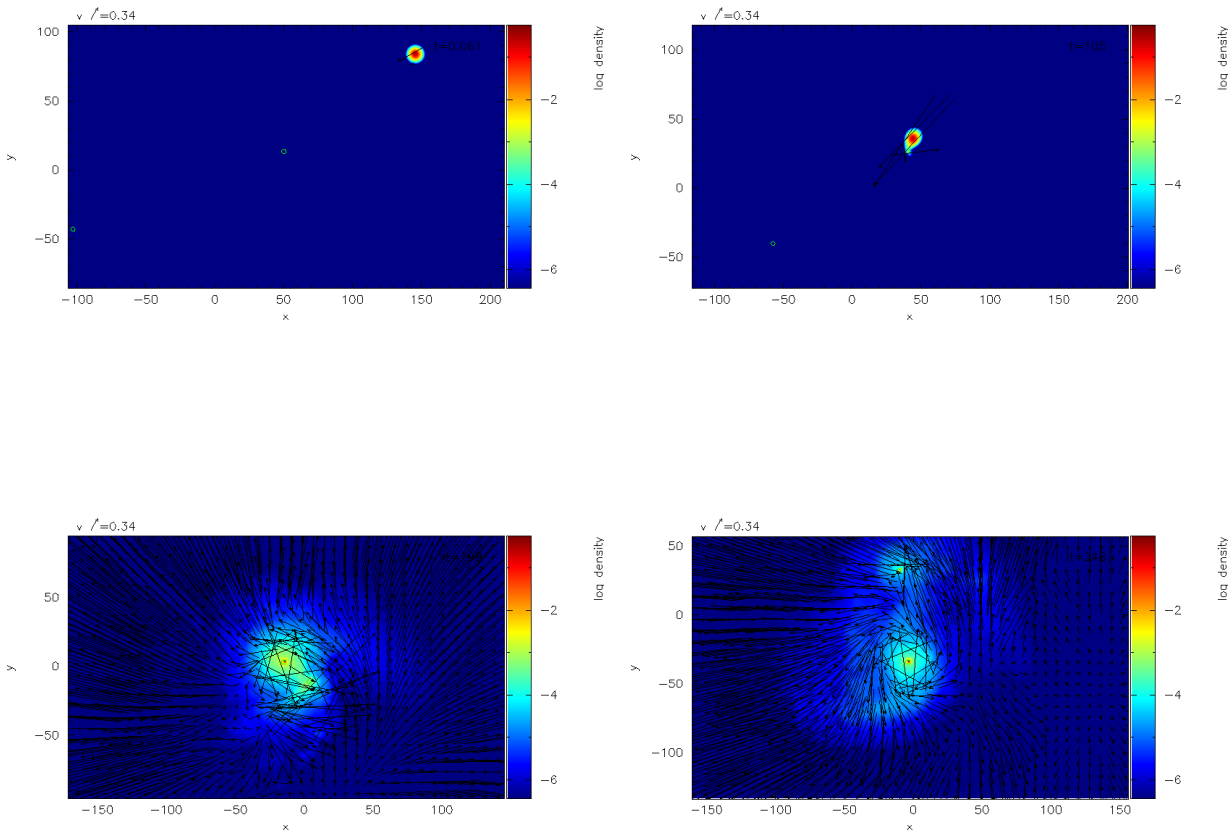
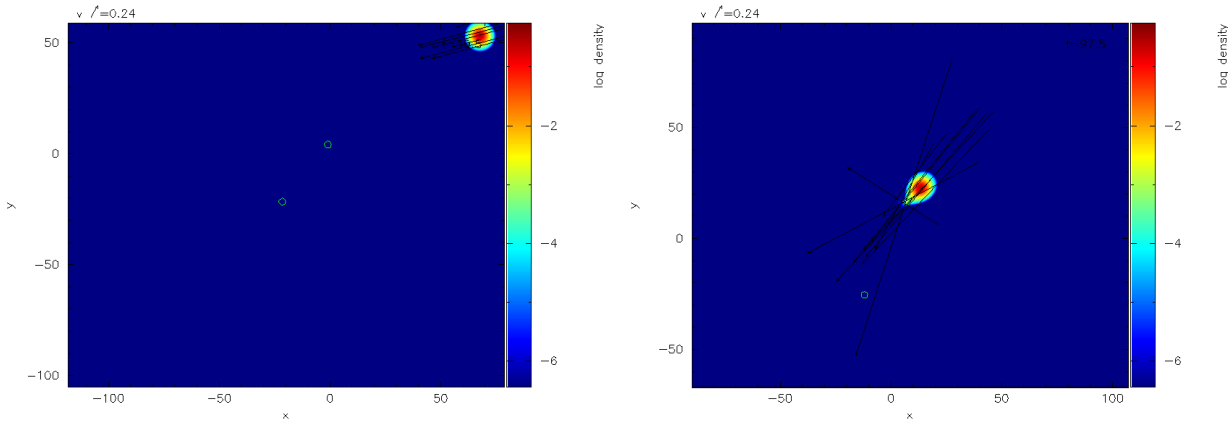


Figure 29: Case #1: An example of no spin flip with velocity vectors overlaid and BH1 visually centered. The colors represent the logarithmic density at each point. The figure depicts the interaction at times 0, 105, 198, and 248 code time units.



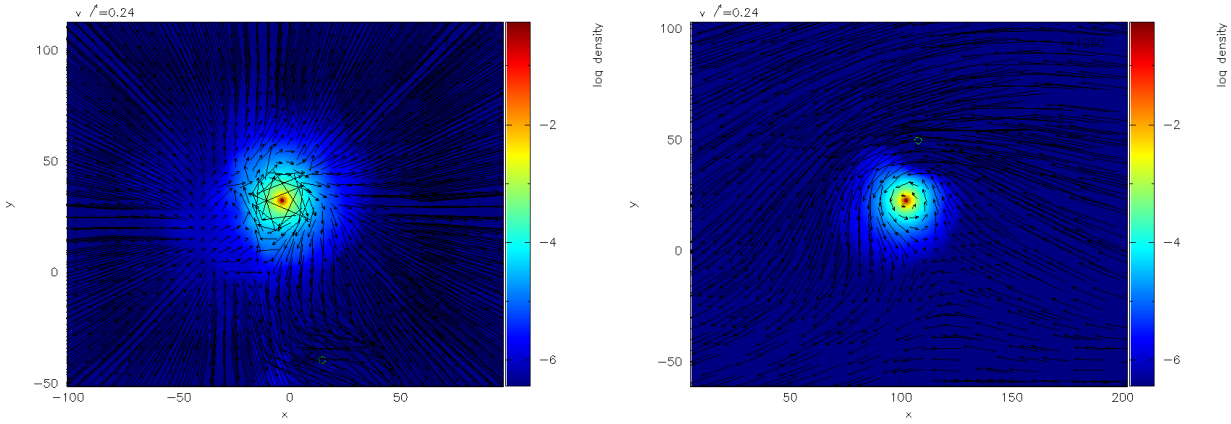


Figure 30: Case #2: An example of spin flip with velocity vectors overlaid and BH1 visually centered. The figure depicts the interaction at times 0, 97.5, 150, and 1250 code time units.

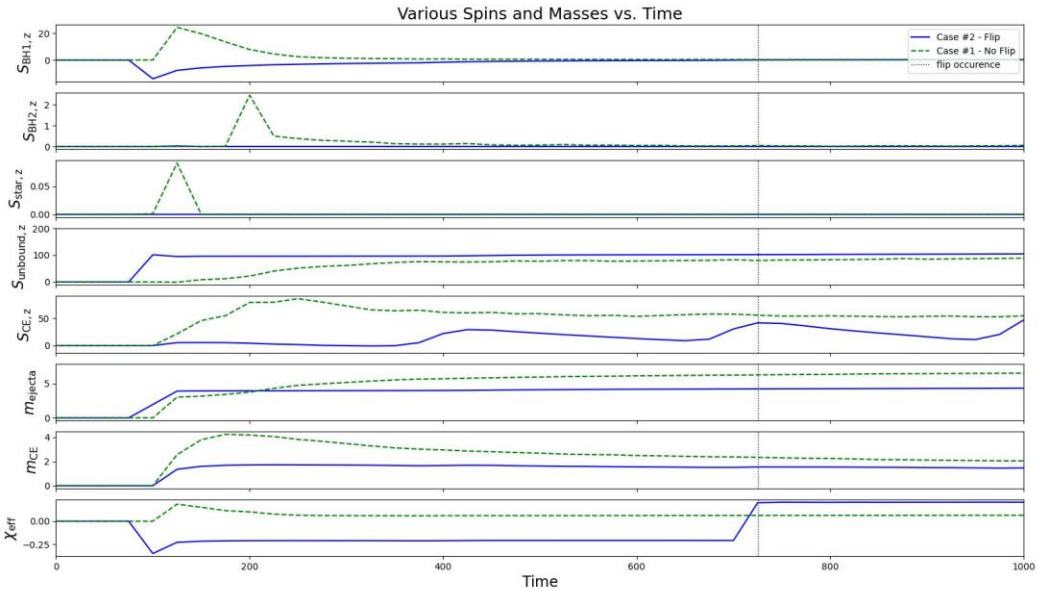


Figure 31: Various spins and masses vs. time for cases #1 (no spin flip) and #2 (spin flip). The most important plot to inspect is χ_{eff} to see the spin flip for case #2. The spins and masses do not relay a cause for my case #2 has a flip and case #1 does not, leading to the belief that this may have been solely based on the orbital rotation parameters. All masses are in units of $M_\odot$, spins in $\sqrt{GM_\odot^3 R_\odot}$, and time in code units.

Seventeen out of the twenty-one relevant cases induce a spin flip, as explained in Table 2. This motivates the findings by the LVK catalog that suggest dynamical three-body interactions have an average final positive χ_{eff} despite their random nature. Post-collision, the BBH angular momentum torques the accretion disks of both BHs to align the spins, giving a final positive χ_{eff}.

4.4 Dynamical Outcomes

Despite the positive χ_{eff} convergence discussed above, these simulations must be proven to be both realistic and theoretically accurate. Analyzing the timescales and aligning the data with theoretical models can accomplish this.

As discussed in section 2.3.5, the encounter and inspiral timescales must align accurately with acceptable values for this globular cluster. There are two scenarios that allow the data to be relevant: 1. $t_{\text{GW}} < 43$ Myr, meaning the BBH will inspiral before a subsequent encounter; 2. $v_{\text{kick}} > v_{\text{escape}}$, meaning the BBH will escape the cluster, making high t_{GW} values relevant. If neither of these criteria are met, then the BBH will have a subsequent encounter, thereby making this data obsolete. Depending on the subsequent encounter, χ_{eff} will change from the final values listed for these simulations. The data that fall under this category cannot be proven to end with positive χ_{eff} before the merger; however, the 100% positive final χ_{eff} rate from this dataset suggests positive final χ_{eff} for any random subsequent collision is almost certain. The LVK Catalog suggests that the four cases with high t_{GW} ($\sim$1 Gyr) and sufficient v_{kick} can be LIGO sources at low redshift, that is the GWs would be detectable and suggest a BBH moving away from the observer slowly. *CMC* data by Anagnostou et al. indicates that dynamically formed BBH mergers are possible both in their host cluster and after ejection; however, only 17% of the mergers were from the latter [30]. The present data set reveals an 18% ejected merger rate and a 9% in-cluster merger rate, with the other 73% of cases being left unknown. Since this data set was not ran for a cluster but rather for separate individual collisions of the same scenario, it cannot be confirmed whether the cases would have aligned properly with the data set from Anagnostou et al.

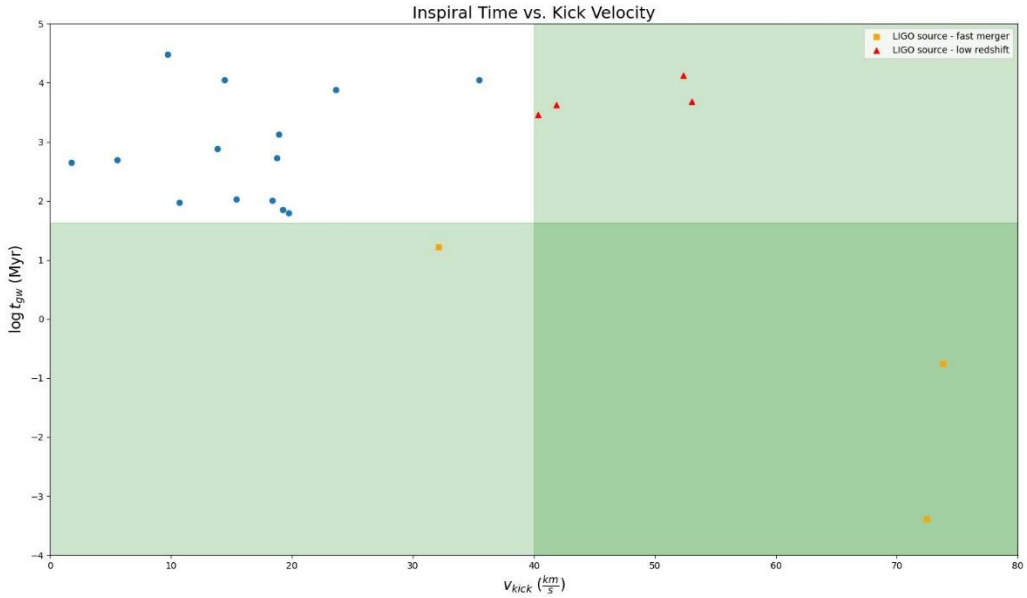


Figure 32: Inspiral time vs. kick velocity for all cases.
The green regions denote cases that will result in a BBH merger before a subsequent encounter. The red triangles denote cases with $v_{\text{kick}} > v_{\text{escape}}$, supporting findings of LIGO sources with low redshift. The orange squares denote cases with $t_{\text{GW}} <$ 43 Myr. The $v_{\text{kick}} = v_{\text{escape}} = 40\frac{\text{km}}{\text{s}}$ boundary is supported in section 2.5.6. The $t_{\text{GW}} = 43$ Myr boundary is supported in section 2.3.5. From this, seven out of twenty-one cases will result in a BBH merger before a subsequent encounter, giving a ~33% success rate.

The problem with the data set as explained above is a lack of cases with either fast enough v_{kick} or short enough t_{GW} after the encounter. A goal of mine is to find which variables have the greatest effect on these variables. As displayed in equation 2.3.9, t_{GW} is dependent on a and e. Plotting equation 2.5.10 for various $\mu * k$ values demonstrate a fit to the SPH data, shown in Figure 33 below. This plot highlights the alignment between data and theory in this realm. Also, it shows that as A increases, $e_{\text{BBH,f}}$ decreases, making the orbit more circular; however, the t_{GW} times do not perfectly align in increasing order from top left to bottom right. This can be attributed to small variations in the outcomes due to the geometry of the interactions. For example, case #1, which has $t_{\text{GW}} = 30{,}734.46$ Myr, is located at the top left of this plot, but the BHs are gravity assisted by the stellar accretion to a large orbit. The variation of points in the bottom right of the plot is caused by differences in their $\mu * k$ value because of more accretion, exemplified by the upper and lower bounds of $\mu * k$ drawn on the plot. Refer to equation 2.5.10 to provide relevance for $\mu * k$.

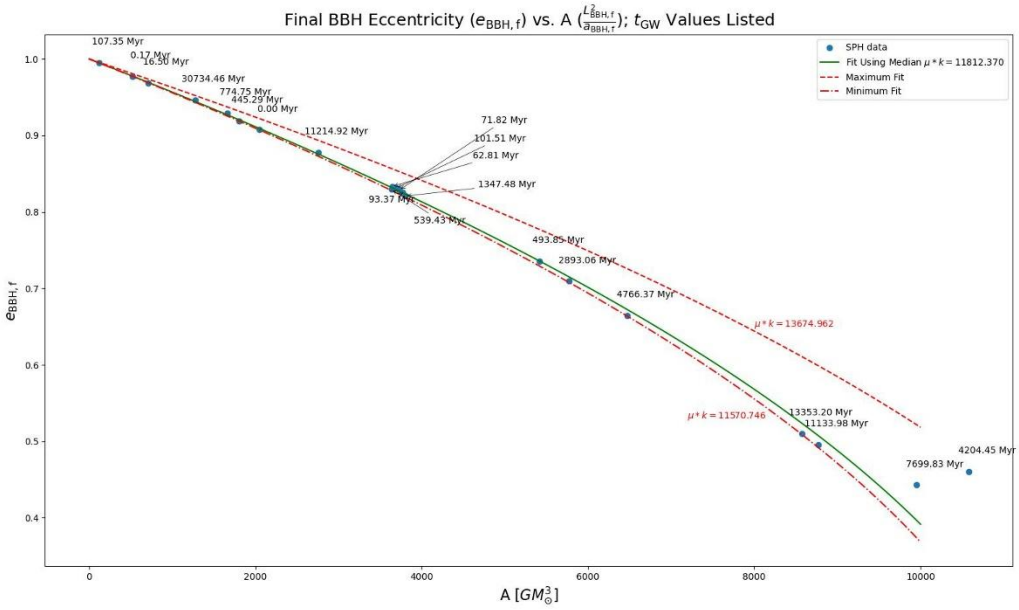


Figure 33: Final BBH eccentricity vs. the composite variable $A = \frac{L^2_{\mathrm{BBH,f}}}{a_{\mathrm{BBH,f}}}$, with SPH data represented as blue dots and equation 2.5.10 as the solid and dashed lines, and t_{GW} values written next to each case.
Due to differences in mass accretion in each case, the $\mu * k$ value is slightly different, especially seen with the two cases farthest to the bottom right of the plot; however, the solid green line uses the median $\mu * k$ value for the dataset, with the red dotted and dashed lines being minimum and maximum boundaries on $\mu * k$. The $\mu * k$ values are in units of $[\mathrm{GM}^3_\odot]$.

A better relationship is the final BBH energy, $E_{\mathrm{BBH,f}}$, and the final BBH angular momentum. As seen by equation 2.5.4, large $E_{\mathrm{BBH,f}}$ will cause small $|a|$ and therefore a tighter orbit, and as seen by equation 2.5.9, small $L_{\mathrm{BBH,f}}$ will cause large $e_{\mathrm{BBH,f}}$ and therefore a more parabolic orbit. These relationships are supported by the data, as shown in Figure 34.

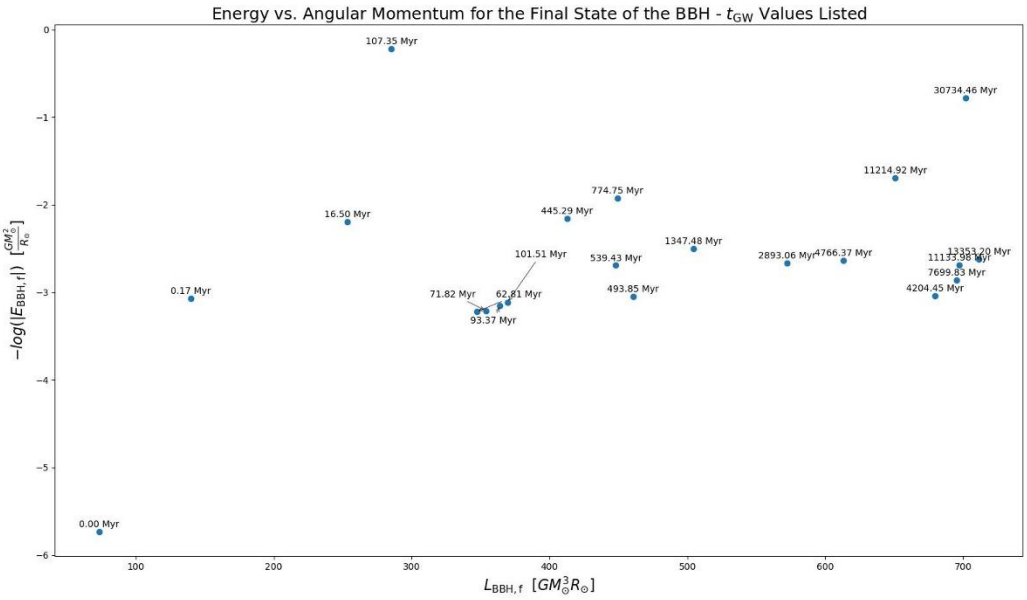


Figure 34: Total BBH energy vs. total BBH angular momentum for all 21 dynamical simulations. Cases with high |energy| and low angular momentum result in the shortest t_{GW}, supporting the theory. The arrows simply point from labels to points because of congestion. A negative of the logarithmic magnitude of the energy is used for plotting purposes since a logarithm of a negative value (which the energy is inherently) is invalid.

When $L_{BBH,f}$ is less than $L_{BBH,i}$, the BBH is effectively tightening because of the r dependence in equation 2.5.2. It is expected to see some positive relationship between the inspiral time and the BBH angular momentum because $L_{BBH,f}$ values should correspond with $t_{GW,f}$ values and similarly between $L_{BBH,i}$ and $t_{GW,i}$. The data aligns with expectations as seen in Figure 35.

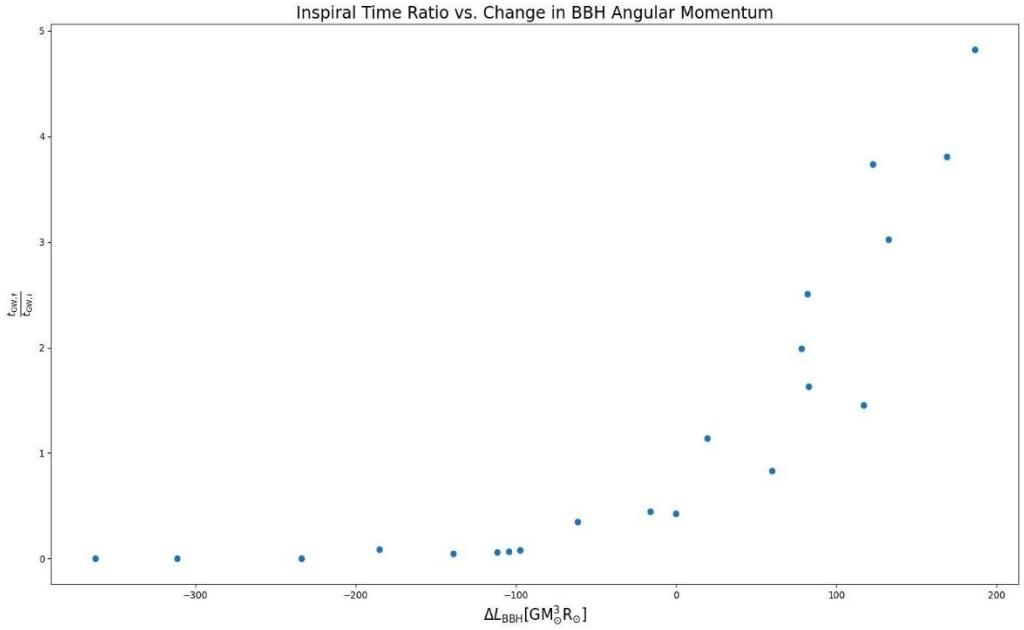


Figure 35: Relationship between the inspiral time ratio and change in BBH angular momentum. Every point is a case. This proves a positive relationship between these two variables which is expected. An inspiral time ratio is used to provide information about the initial state of the case and how this relates to the final state. Although this ratio largely depends on $t_{\mathrm{GW,f}}$ due to consistent $t_{\mathrm{GW,i}}$ values, $t_{\mathrm{GW,i}}$ is not constant.

The final goal is to find some relationship between an initial parameter and the final t_{GW} so that any future research on this topic can be focused on that parameter space. The best connection found for this dataset is with the initial total angular momentum of the system, $L_{\mathrm{tot,i}}$. The same inspiral time ratio used in Figure 35 is used in Figure 36 to show a positive correlation with $L_{\mathrm{tot,i}}$. This plot indicates that low $L_{\mathrm{tot,i}}$ correlates with long initial inspiral time, short final inspiral time, or both. Although a short initial inspiral time could overpower a short final inspiral time in this parameter, this is proven unlikely from the large $t_{\mathrm{GW,i}}$ values in Table 2, visualized for cases #17, #21, and #22 in Figure 36.

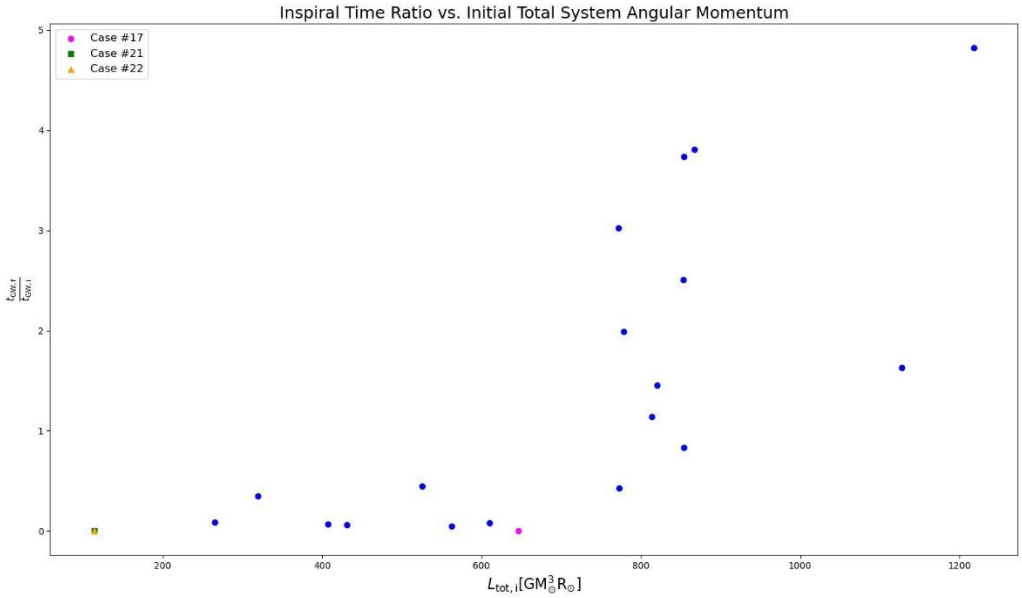


Figure 36: Relationship between the inspiral ratio and initial total system angular momentum. Cases #17, #21, and #22 are highlighted as the three cases with $t_{\mathrm{GW}} < 43$ Myr, and help support the hypothesis that short $t_{\mathrm{GW,i}}$ will not override short $t_{\mathrm{GW,f}}$ values in the ratio.

5. Conclusion

This project aimed to discover which parameters cause positive spin alignment between pre-MS stars and dynamically formed BBHs in globular clusters, including discussion about the orbital configurations, masses, and angular momenta of the bodies in the system. All twenty-one cases that resulted in a bound BBH yielded positive final χ_{eff}, which supports findings from Kıroğlu et al [4]. Seventeen of these undergo a spin flip from the torque of the BBH orbit at some point in the simulation. Six of these seventeen spin flip cases involved a BBH orbit flip after the first interaction with the star, such as an initially clockwise orbit becoming counterclockwise afterward.

For the mass ratio studied, spin flips occurred without exception for any case that did not have an initial positive χ_{eff}, which can be attributed to the more massive BBH exerting a stronger torque on the accretion disk than the possible torque from the accretion disk. An initial

negative χ_{eff} was found in cases where the star passed above the clockwise rotating BBH, with the opposite found when the star passed underneath the BBH; however, the contrary happened if a BBH orbit flip occurred.

A simple three-body integrator code was used to determine which regions of parameter space would lead to a star-BBH collision for scenario #2. Although SPH cases were not chosen using random number generation, the orbital configurations chosen proved to be generally random. Also, although the probability of collision for the parameter space was similar on average, the highest probabilities are found for coplanar cases, where the inclination angle is either $0\,°$ or $180\,°$, which corroborates the reduction of one degree of freedom in the spatial dimension.

In the search for justifying this data, the inspiral and encounter timescales, as well as the escape and kick velocities, became important factors in deciding the relevance of all cases. Only three out of the twenty-one valid cases resulted in $t_{\text{GW,f}} < t_{\text{enc}} = 43$ Myr, and four separate cases resulted in $v_{\text{kick}} > v_{\text{escape}} = 40\,\frac{\text{km}}{\text{s}}$, with all final outcomes being represented except DTDEs. This makes a total of seven out of twenty-one cases that will, directly from this interaction, produce GWs that are connected to this, and only this, interaction. This is a healthy percentage of cases with first-time interactions leading to BBH mergers, but since not all interactions lead to BBH mergers, it may be tough to distinguish between which LIGO sources have gone through one or multiple interactions before the merger.

5.1 Future Work

This project has paved the way for many more interesting topics to be studied. BBH interactions are very complex, and the geometrical parameter space is huge. The first path would be to study scenarios #1, #3, and #4 to search for similar or different outcomes. Scenarios #1 and #3 use MS stars, but scenario #4 uses an RG star which is also not modeled well. Improving this model and exploring a similar parameter space for these other scenarios will be useful for comparing outcomes between models.

Another similar step would be to allow all simulations for scenario #2, and others, to run to a set final time. Since all the simulations have various outcomes, some would seem to “end” quicker than others; however, it is hard to define an end without using a definite final time. This

is a small addition to this work that, with the extra time needed, could benefit the conclusions. Along with this step it would be wise to continue filling in the parameter space by running new simulations for scenario #2. Since this would take lots of computing time, a new method would be to try teaching a machine learning model to read in the current data and to guess which areas in parameter space should be focused on.

Finally, to continue with an idea mentioned in section 5, studying a collision tree for a specific BBH from creation until merger may be interesting. By using *CMC* data, the history of a BBH can be estimated and then *StarSmasher* can be used to simulate more accurate models. Kremer et al. (2020) studied the upper BH mass gap with a similar technique [31].

Bibliography

[1] J. M. Lopez, A. Batta, E. Ramirez-Ruiz, I. Martinez and J. Samsing, "Tidal Disruptions of Stars by Binary Black Holes: Modifying the Spin Magnitudes and Directions of LIGO Sources in Dense Stellar Environments," *The Astrophysical Journal,* vol. 877, no. 1, p. 56, 2019.

[2] M. Fishbach, C. Kimball and V. Kalogera, "Limits on Hierarchical Black Hole Mergers from the Most Negative chi_eff Systems," *The Astrophysical Journal,* vol. 935, no. 2, pp. 1-7, 2022.

[3] F. Kiroğlu and e. al., *Spin-Orbit Alignment of Black Hole Binaries through Accretion in Young Star Clusters,* In Preparation, 2024.

[4] F. Kiroğlu, J. C. Lombardi Jr., K. Kremer, H. D. Vanderzyden and F. A. Rasio, "Spin-Orbit Alignment in Merging Binary Black Holes Following Collisions with Massive Stars," *The Astrophysical Journal,* 2025.

[5] B. W. Carroll and D. A. Ostlie, An Introduction to Modern Astrophysics, Addison Wesley Publishing Company, 2007.

[6] E. Gaburov, J. C. J. Lombardi and S. Portegies Zwart, "Onthe onset of runaway stellar collisions in dense star clusters– II. Hydrodynamics of three-body interactions," *Monthly Notices of the Royal Astronomical Society,* pp. 105-126, 2009.

[7] European Southern Observatory, "Hertzsprung-Russell Diagram," 19 June 2007. [Online]. Available: https://www.eso.org/public/images/eso0728c/. [Accessed 29 October 2024].

[8] H. Wirth, J. Haas, L. Šubr, T. Jerabkova, Z. Yan and P. Kroupa, "Failed supernova explosions increase the duration of stellar formation in globular clusters," *Astronomy & Astrophysics,* vol. 691, p. A227, 2024.

[9] L. Portinari, C. Chiosi and A. Bressan, "Galactic chemical enrichment with new metallicity dependant stellar yields," *Astronomy and Astrophysics,* vol. 334, pp. 505-539, 1998.

[10] J. Fregeau, P. Cheung, S. Portegeis Zwart and F. Rasio, "Stellar collisions during binary-binary and binary-single star interactions," *Monthly Notices of the Royal Astronomical Society,* vol. 352, no. 1, pp. 1-19, 2004.

[11] I. Mandel and A. Farmer, "Merging stellar-mass binary black holes," *Physics Reports,* vol. 955, pp. 1-24, 2022.

[12] C. F. A. Gibson, F. Kiroğlu, J. C. Lombardi Jr., S. C. Rose, H. D. Vanderzyden, B. Mockler, M. Gallegos-Garcia, K. Kremer, E. Ramirez-Ruiz and F. A. Rasio, "Formation of Stripped Stars from Stellar Collisions in Galactic Nuclei," *The Astrophysical Journal,* vol. 980, no. 1, p. 19, 2025.

[13] P. Peters, "Gravitational Radiation and the Motion of Two Point Masses," *Physical Review Journals,* vol. 136, no. 4B, pp. B1224--B1232, 1964.

[14] E. Hecht, Optics, Pearson, 2017.

[15] "LIGO's Interferometer," LIGO Caltech, [Online]. Available: https://www.ligo.caltech.edu/page/ligos-ifo. [Accessed 22 10 2024].

[16] A. Returns, "Section 4.3 - The Six Orbital Elements," [Online]. Available: https://www.astronomicalreturns.com/p/section-43-six-orbital-elements.html. [Accessed 1 11 2024].

[17] S. T. Marion and T. J. B., Classical Dynamics of Particles and Systems, Brooks/Cole Publishing Company, 2004.

[18] T. A. Moore, Six Ideas that Shaped Physics: Unit R - The Laws of Physics are Frame-Independent, New York: McGraw-Hill, 2003.

[19] O. Y. Gnedin, H. Zhao, J. E. Pringle and M. S. Fall, "THE UNIQUE HISTORY OF THE GLOBULAR CLUSTER ω CENTAURI," *The Astrophysical Journal,* vol. 568, no. 1, pp. L23-L26, 2018.

[20] C. R. a. S. Coughlin, "The Cluster Monte Carlo Code, CMC," 2021. [Online]. Available: https://clustermontecarlo.github.io/CMC-COSMIC/. [Accessed 4 11 2024].

[21] M. H. Henon, "The Monte Carlo Method," *Astrophysics and Space Science,* vol. 14, pp. 151-167, 1971.

[22] G. Buldgen, A. Noels, V. A. Baturin, A. V. Oreshina, S. V. Ayukov, R. Scuflaire, A. M. Amarsi and N. Grevesse, "Helioseismic determination of the solar metal mass fraction," *Astronomy & Astrophysics,* vol. 687, no. A57, p. 15, 2024.

[23] B. Paxton and e. al., "MODULES FOR EXPERIMENTS IN STELLAR ASTROPHYSICS (MESA)," *The Astrophysical Journal,* vol. 192, no. 1, p. 3, 2010.

[24] T. M. Team, "MESA," 2024. [Online]. Available: https://docs.mesastar.org/en/24.08.1/about.html. [Accessed 4 11 2024].

[25] F. Caputo and S. Cassisi, "Global metallicity of globular cluster stars from colour-magnitude diagrams," *Monthly Notices of the Royal Astronomical Society,* vol. 333, no. 4, pp. 828-834, 2002.

[26] E. Chambers and H. Vanderzyden, *An Analysis of Collisions between Main Sequence Stars and Binary Black Holes [PowerPoint Presentation],* Meadville, 2023.

[27] S. Karekal, R. Das, L. Mosse and P. W. Cleary, "Application of a mesh-free continuum method for simulation of rock caving processes," *International Journal of Rock Mechanics and Mining Sciences,* vol. 48, no. 5, pp. 703-711, 2011.

[28] D. Price, "Visualization of smoothed particle hydrodynamics data using splash," 2004. [Online]. Available: https://splash-viz.readthedocs.io/en/latest/refs.html. [Accessed 13 November 2024].

[29] K. Kremer, J. C. Lombardi Jr., W. Lu, A. L. Piro and F. A. Rasio, "Hydrodynamics of Collisions and Close Encounters between Stellar Black Holes and Main-sequence Stars," *The Astrophysical Journal,* vol. 933, no. 203, pp. 1-18, 2022.

[30] O. Anagnostou, M. Trenti and A. Melatos, "Dynamically Formed Black Hole Binaries: In-Cluster Versus Ejected Mergers," *Publications of the Astronomical Society of Australia,* vol. 37, pp. 1-22, 2020.

[31] K. Kremer, M. Spera, D. Becker, S. Chatterjee, U. N. Di Carlo, G. Fragione, C. L. Rodriguez, C. S. Ye and F. A. Rasio, "Populating the Upper Black Hole Mass Gap through Stellar Collisions in Young Star Clusters," *The Astrophysical Journal,* vol. 903, no. 1, p. 18, 2020.

Appendix A

Three-Body Integrator Python Code

Section 3.3 describes the use of three-body integration with a Python code before choosing which orbital parameters to use in dynamical *StarSmasher* simulations. On page 74, variables *numi*, *num_trueanomaly*, *num_argperi*, and *num_longitude* provide the code how many steps to loop through the inclination, true anomaly, argument of periapsis, and longitude of the ascending node angles, from $-180°$ to $180°$. Larger values produce more data points, as well as longer runtime. For this project, a step size of fifteen was used for each angle. The *CMC* data file provided by Fulya Kıroğlu had columned variables, with each column having an index found by the comments on page 72.

```
"""Three-body integrator tool for pre-collision trajectories.
Created by Dr. James C. Lombardi, Jr. in the Summer of 2023 during URSCA for Hans
Vanderzyden '25 and Emma Chambers '24.
Minor edits by Hans Vanderzyden.
"""

import numpy as np
import sys

data = input("Enter a line of data from the binary_single.dat file: \n")

# Split the line of data into individual elements
elements = data.split()

# Accoording to an email from Fulya on June 6, 2023, these are what the data
mean:
#0.path_ID
#1.time : time of the collision
#2.m_sin : mass
#3.m_bin1
#4.m_bin2
#5.R_sin #stellar radius
#6.R_bin1
#7.R_bin2
#8.k_sin :stellar type (k=14 : BH, k<=1: MS, 2<=k<10 : Giant)
#9.k_bin1
#10.k_bin2
#11.a_bin(AU) :semi-major axis before collision
#12.e_bin :eccentricity before collision
#13.v_inf(km/s) :velocity at infinity
#14.b(rsun) :impact parameter
#15.id_sin
#16.id_bin1
#17.id_bin2
#18.m1_col :mass of the colliding object 1
#19.m2_col :mass of the colliding object 2
#20.k1_col: :stellar type of  the colliding object 1
#21.k2_col : stellar type of  the colliding object 2
#22.a_fin : semi-major axis of the binary after collision
#23.e_fin: eccentricity of the binary after collision
#24.rperi(rsun) :pericenter distance ( I calculated this using the impact
parameter and v_inf. Hopefully, it is correct)

# Open a file to write and then redirect the standard output to the file
with open("collision_parameters_output.txt", 'w') as file:
```

```
    sys.stdout = file

    if elements[8] == "14":
        print("The single intruder object should be a star, not a black hole")
        raise SystemExit

    # Assign the required variables
    am1 = float(elements[2])
    bbh_m1 = float(elements[3])
    bbh_m2 = float(elements[4])
    radius1 = float(elements[5])
    bbh_semimajoraxis_AU = float(elements[11])
    bbh_e0 = float(elements[12])
    vinf_kps = float(elements[13])
    impactparameter = float(elements[14])
    m1_col = float(elements[18])
    m2_col = float(elements[19])


    file.write("The colliding objects are ")
    if m1_col == am1:
        file.write("the intruder star and ")
        icol1 = 1
    elif m1_col == bbh_m1:
        file.write("binary component 1 and ")
        icol1 = 2
    elif m1_col == bbh_m2:
        file.write("binary component 2 and ")
        icol1 = 3
    if m2_col == am1:
        file.write("the intruder star.")
        icol2 = 1
    elif m2_col == bbh_m1:
        file.write("binary component 1.")
        icol2 = 2
    elif m2_col == bbh_m2:
        file.write("binary component 2.")
        icol2 = 3
    if icol1 > icol2:
        icol1, icol2 = icol2, icol1

    if icol1 != 1:
        file.write("For now, the intruder star must be part of the collision.")
        raise SystemExit
```

```
    # Display the assigned variables
    print("am1, bbh_m1, bbh_m2 [Msun] =", am1, bbh_m1, bbh_m2)
    print("radius1 =", radius1)
    print("bbh_semimajoraxis [AU] =", bbh_semimajoraxis_AU)
    print("bbh_e0 =", bbh_e0)
    print("vinf_kps =", vinf_kps)
    print("impactparameter =", impactparameter)

    # Write to file
    file.write("am1, bbh_m1, bbh_m2 [Msun] = " + str(am1) + ", " + str(bbh_m1) +
", " + str(bbh_m2) + "\n")
    file.write("radius1 = " + str(radius1) + "\n")
    file.write("bbh_semimajoraxis [AU] = " + str(bbh_semimajoraxis_AU) + "\n")
    file.write("bbh_e0 = " + str(bbh_e0) + "\n")
    file.write("vinf_kps = " + str(vinf_kps) + "\n")
    file.write("impactparameter = " + str(impactparameter) + "\n")

    # Control how finely you want to explore parameter space of the four unset
degrees of freedom:
    numi = 15 # number of different inclination angles to consider
    num_trueanomaly = 15 # number of different true anomaly values to consider
    num_argperi = 15 # number of different argument of periapsis values to
consider
    num_longitude = 15 # number of different longitudes of ascending node values
to consider

    step_trueanomaly = -2*np.pi/num_trueanomaly
    step_argperi = -2*np.pi/num_argperi
    step_longitude = -2*np.pi/num_longitude

    verbosity = 0 # set to 0 for the key output only.  Make it larger for more
output to the screen

    bbh_semimajoraxis=bbh_semimajoraxis_AU*149597870700/6.957e8 # converted to
R_sun

    # Function to calculate the gravitational accelerations of the point masses
    def gravitational_acceleration(r1, r2, r3):

        # Calculate the distances between the point masses
        d12 = np.linalg.norm(r1 - r2)
        d13 = np.linalg.norm(r1 - r3)
        d23 = np.linalg.norm(r2 - r3)

        # Calculate the gravitational forces
```

```
        f12 = G * (am1 * bbh_m1) / d12**3 * (r2 - r1)
        f13 = G * (am1 * bbh_m2) / d13**3 * (r3 - r1)
        f23 = G * (bbh_m1 * bbh_m2) / d23**3 * (r3 - r2)

        # Calculate the accelerations
        a1 = (f12 + f13) / am1
        a2 = (-f12 + f23) / bbh_m1
        a3 = (-f13 - f23) / bbh_m2

        dta = 0.001*min(d12/np.linalg.norm(a1 - a2),d13/np.linalg.norm(a1 -
a3),d23/np.linalg.norm(a2 - a3))**0.5
        dtv = 0.001*min(d12/np.linalg.norm(v1 - v2),d13/np.linalg.norm(v1 -
v3),d23/np.linalg.norm(v2 - v3))
        dt = min(dta, dtv)

        return a1, a2, a3, dt, d12, d13, d23

    gravconst = 6.67390e-8     # Newton's gravitational constant G in cgs units
    runit = 6.9599e10          # number of cm in the unit of length.  6.9599d10
is solar radius.
    munit = 1.9891e33          # number of g in unit of mass.  1.9891d33 is solar
mass.
    vunit = np.sqrt(gravconst*munit/runit)*1e-5 # This is the velocity unit in
km/s
    G = 1  # Gravitational constant

    am2 = bbh_m1+bbh_m2
    k_bin=bbh_m1*bbh_m2
    mu_bin=k_bin/(bbh_m1+bbh_m2)
    bbh_rp=bbh_semimajoraxis*(1-bbh_e0)
    bbh_eorb0=-0.5*k_bin/bbh_semimajoraxis
    bbh_vinf2=2*bbh_eorb0/mu_bin
    bbh_semilatusrectum=bbh_rp*(1+bbh_e0)

    rT1 = (bbh_m1/am1)**(1/3)*radius1
    rT2 = (bbh_m2/am1)**(1/3)*radius1
    rT = (am2/am1)**(1/3)*radius1
    sep0 = max(6*bbh_semimajoraxis, 10*rT)
    vinf = vinf_kps / vunit
    vinf2 = vinf**2
    xx=(am1+am2)/(vinf2*impactparameter)
    rp=impactparameter/(xx+np.sqrt(1+xx**2))
    k=am1*am2
    mu=am1*am2/(am1+am2)
```

```
    eorb0=0.5*mu*vinf2
    semimajoraxis=-0.5*k/eorb0
    e0=1-rp/semimajoraxis
    semilatusrectum=rp*(1+e0)

    if verbosity > 0:
        print('velocity unit vunit=',vunit,'km/s')
        print('bbh_rp=',bbh_rp,'bbh_v_inf2=',bbh_vinf2,'bbh_semimajoraxis=',bbh_s
emimajoraxis)
        print('bbh_e_orb=',bbh_eorb0)
        print('initial separation=', sep0)
        print('vinf2=', vinf2)
        print('dimensionless parameter x=',xx)
        print('rp=', rp)
        print('impactparameter=',impactparameter,'v_inf2=',vinf2,'semimajoraxis='
,semimajoraxis)
        print('e_orb=',eorb0)

    #     equation (8.41) of marion and thornton
    costheta = (semilatusrectum/sep0-1)/e0
    if abs(costheta) > 1:
        print('costheta problem')
        raise SystemExit

    #     equation (8.40) of marion and thornton
    ltot = np.sqrt(semilatusrectum*mu*k)
    #     equation (8.10) of marion and thornton
    thetadot = ltot/mu/sep0**2
    #     equation (8.40) of marion and thornton
    eorb0check = (e0**2-1)*mu*k*k/(ltot*ltot)*0.5
    if verbosity > 0:
        print('1st simple check:',eorb0,eorb0check)

    theta=-np.arccos(costheta)
    sinthetacheck = np.sin(theta)
    sintheta = -np.sqrt(1-costheta**2)
    if abs(sintheta-sinthetacheck) > 1e-13:
        print('2nd simple check fails',sintheta,sinthetacheck,abs(sintheta-
sinthetacheck))
        raise SystemExit
    #     the minus signs on the position and velocity component equations
    #     have been chosen so that the separation vector r equals r2-r1,
    #     *not* r1-r2 as in marion and thornton.  this was done so that the
    #     code would give the same initial conditions as twostars.f when the
    #     eccentricity is 1
```

```
    deltax1 = -am2/(am1+am2)*sep0*costheta
    deltay1 = -am2/(am1+am2)*sep0*sintheta
    deltax2 = am1/(am1+am2)*sep0*costheta
    deltay2 = am1/(am1+am2)*sep0*sintheta
    #     differentiating eqn. 8.41
    rdot=semilatusrectum/(1+e0*costheta)**2*e0*sintheta*thetadot
    #     another expr. for rdot (using eqn. 8.14) and compare
    rdotcheck=-np.sqrt((eorb0-0.5*ltot**2/mu/sep0**2+k/sep0)/0.5/mu)
    #if(rdot.ne.rdot)rdot=rdotcheck

    deltavx1=am2/(am1+am2)*(sep0*sintheta*thetadot-rdot*costheta)
    deltavy1=am2/(am1+am2)*(-sep0*costheta*thetadot-rdot*sintheta)
    deltavx2=am1/(am1+am2)*(-sep0*sintheta*thetadot+rdot*costheta)
    deltavy2=am1/(am1+am2)*(sep0*costheta*thetadot+rdot*sintheta)

    xcm=(am1*deltax1+am2*deltax2)/(am1+am2)
    ycm=(am1*deltay1+am2*deltay2)/(am1+am2)
    vxcm=(am1*deltavx1+am2*deltavx2)/(am1+am2)
    vycm=(am1*deltavy1+am2*deltavy2)/(am1+am2)

    if verbosity > 0:
        print('semilatusrectum=',semilatusrectum,' mu=',mu,' sep0=',sep0,'
e0=',e0)
        print('cos=',costheta,' sin=',sintheta)
        print('rdot(from semilatusrectum): ',rdot,'  rdot(from e): ',rdotcheck)
        print('initially..... star : x=',deltax1,',y=',deltay1)
        print('                      vx=',deltavx1,',vy=',deltavy1)
        print('center of mass of binary: x=',deltax2,',y=',deltay2)
        print('                      vx=',deltavx2,',vy=',deltavy2)
        print('center of mass position (should be zeros):',xcm,ycm)
        print('center of mass velocity (should be zeros):',vxcm,vycm)

    # We've determined initial positions and velocities (treating so far the
binary as a single object)
    # Now's a good time to do some sanity checks
    ak=am1*am2
    amu=am1*am2/(am1+am2)
    r = np.sqrt((deltax1-deltax2)**2 + (deltay1-deltay2)**2)
    eorb0check = 0.5*(am1*(deltavx1**2+deltavy1**2) +
am2*(deltavx2**2+deltavy2**2)) - am1*am2/r
    altotint = am1*(deltax1*deltavy1 - deltay1*deltavx1) + am2*(deltax2*deltavy2
- deltay2*deltavx2)
    e0check = np.sqrt(1 + 2*eorb0check*altotint**2/amu/ak**2)
    semilatusrectumprime = r+e0*(deltax2-deltax1)
    if abs(r/sep0-1) > 1e-8:
```

```
        print('sep0 problem',r,sep0)
        raise SystemExit
    if abs(eorb0check-eorb0) > 1e-8:
        print('eorb0 problem',eorb0check,eorb0)
        raise SystemExit
    if abs(altotint/ltot-1) > 1e-8:
        print('angular momentum problem',altotint,ltot)
        raise SystemExit
    if abs(e0check-e0) > 1e-7:
        print('eccentricity problem',e0check,e0)
        raise SystemExit
    if abs(semilatusrectumprime/semilatusrectum-1) > 1e-8:
        print('semilatusrectum problem',semilatusrectumprime,semilatusrectum)
        raise SystemExit

    for bbh_cosi in np.linspace(-1,1,numi):
        bbh_inclination=np.arccos(bbh_cosi) # relatve to the orbit of the
intruder star (0 is coplanar)
        bbh_inclination_degrees = bbh_inclination * 180 / np.pi
        # https://youtu.be/N_njPJYaXaU?t=1983 contains a nice discussion of
orbital elements
        for bbh_trueanomaly in np.arange(np.pi,-np.pi,step_trueanomaly):
            bbh_trueanomaly_degrees = bbh_trueanomaly * 180 / np.pi
            # bbh_trueanomaly = angle between -pi and pi radians giving how far
past periapsis black hole binary is initially
            # bbh_trueanomaly controls the initial phase of the orbit.

            # Think of a vector pointing from the center of mass of the binary to
the periapsis position.
            # This vector should be able to point anywhere in space to be able to
treat all cases.
            # Together, the angles bbh_argperi and bbh_longitude allow this
vector to point anywhere.
            for bbh_argperi in np.arange(np.pi, -np.pi, step_argperi):
                #bbh_argperi = argument of periapsis
                bbh_argperi_degrees = bbh_argperi * 180 /np.pi
                for bbh_longitude in np.arange(np.pi, -np.pi, step_longitude):
                    # vary longitude of the ascending node
                    bbh_longitude_degrees = bbh_longitude * 180 / np.pi

                    file.write("----------------------------------------------
---------------------------------------- \n")
                    file.write(f"m{am1}_i{round(bbh_inclination_degrees)}_a{round
(bbh_trueanomaly_degrees)}_p{round(bbh_argperi_degrees)}_l{round(bbh_longitude_de
grees)} : i={round(bbh_inclination_degrees)} deg,
```

```
trueanomaly={round(bbh_trueanomaly_degrees)} deg,
argperi={round(bbh_argperi_degrees)} deg,
longitude={round(bbh_longitude_degrees)} deg \n")

                    #     equation (8.41) of marion and thornton
                    #     costheta = (bbh_semilatusrectum/bbh_sep0-1.d0)/bbh_e0
                    theta=bbh_trueanomaly # true anomaly should be from -pi to
+pi
                    costheta=np.cos(theta)
                    bbh_sep0=bbh_semilatusrectum/(1+bbh_e0*costheta)

                    #     equation (8.40) of marion and thornton
                    bbh_ltot = np.sqrt(bbh_semilatusrectum*mu_bin*k_bin)
                    #     equation (8.10) of marion and thornton
                    thetadot = bbh_ltot/mu_bin/bbh_sep0**2
                    #     equation (8.40) of marion and thornton
                    bbh_eorb0check = (bbh_e0**2-
1)*mu_bin*k_bin*k_bin/(bbh_ltot*bbh_ltot)*0.5
                    if verbosity >
0:
                        print('1st simple bbh check:',bbh_eorb0,bbh_eorb0check)

                    sintheta = np.sin(theta)
                    sinthetacheck = np.sqrt(1-
costheta**2)
                    if abs(abs(sintheta)-sinthetacheck ) > 1.e-13:
                        print('2nd simple bbh check
fails',sintheta,sinthetacheck)
                        raise SystemExit


                    if verbosity >
0:
                        print('bbh semilatusrectum=',bbh_semilatusrectum,' bbh
mu=',mu_bin,' bbh_sep0=',bbh_sep0,' bbh_e0=',bbh_e0)
                        print('bbh cos=',costheta,' sin=',sintheta)
                    #     the minus signs on the position and velocity component
equations
                    #     have been chosen so that the separation vector r equals
r2-r1,
                    #     *not* r1-r2 as in marion and thornton.  this was done
so that the
                    #     code would give the same initial conditions as
twostars.f when the
                    #     eccentricity is 1
```

```
                    bbh_deltax1 = -bbh_m2/(bbh_m1+bbh_m2)*bbh_sep0*costheta
                    bbh_deltay1 = -bbh_m2/(bbh_m1+bbh_m2)*bbh_sep0*sintheta
                    bbh_deltax2 = bbh_m1/(bbh_m1+bbh_m2)*bbh_sep0*costheta
                    bbh_deltay2 = bbh_m1/(bbh_m1+bbh_m2)*bbh_sep0*sintheta
                    #     differentiating eqn. 8.41
                    rdot=bbh_semilatusrectum/(1+bbh_e0*costheta)**2*bbh_e0*sinthe
ta*thetadot
                    #     another expr. for rdot (using eqn. 8.14) and
compare
                    rdotcheck=np.sqrt((bbh_eorb0-
0.5*bbh_ltot**2/mu_bin/bbh_sep0**2+k_bin/bbh_sep0)/0.5/mu_bin)
                    bbh_deltavx1=bbh_m2/(bbh_m1+bbh_m2)*(bbh_sep0*sintheta*thetad
ot-rdot*costheta)
                    bbh_deltavy1=bbh_m2/(bbh_m1+bbh_m2)*(-
bbh_sep0*costheta*thetadot-rdot*sintheta)
                    bbh_deltavx2=bbh_m1/(bbh_m1+bbh_m2)*(-
bbh_sep0*sintheta*thetadot+rdot*costheta)
                    bbh_deltavy2=bbh_m1/(bbh_m1+bbh_m2)*(bbh_sep0*costheta*thetad
ot+rdot*sintheta)
                    xcm=(bbh_m1*bbh_deltax1+bbh_m2*bbh_deltax2)/(bbh_m1+bbh_m2)
                    ycm=(bbh_m1*bbh_deltay1+bbh_m2*bbh_deltay2)/(bbh_m1+bbh_m2)
                    vxcm=(bbh_m1*bbh_deltavx1+bbh_m2*bbh_deltavx2)/(bbh_m1+bbh_m2
)
                    vycm=(bbh_m1*bbh_deltavy1+bbh_m2*bbh_deltavy2)/(bbh_m1+bbh_m2
)
                    if verbosity > 0:
                        print('bbh rdot(from semilatusrectum):
',rdot,'  magnitude of bbh rdot(from e): ',rdotcheck)
                        print('Before rotation, compact object 1 starts with
(relative to binary c.o.m.):')
                        print('                    x=',bbh_deltax1,',
y=',bbh_deltay1)
                        print('                   vx=',bbh_deltavx1,',vy=',bbh_d
eltavy1)
                        print('Before rotation, compact object 2 starts with
(relative to binary c.o.m.):')
                        print('                    x=',bbh_deltax2,',
y=',bbh_deltay2)
                        print('                   vx=',bbh_deltavx2,',vy=',bbh_d
eltavy2)
                        print('bbh center of mass position (should be
zeros):',xcm,ycm)
                        print('bbh center of mass velocity (should be
zeros):',vxcm,vycm)
```

```
                    altotint = bbh_m1*(bbh_deltax1*bbh_deltavy1 -
bbh_deltay1*bbh_deltavx1) + bbh_m2*(bbh_deltax2*bbh_deltavy2 -
bbh_deltay2*bbh_deltavx2)
                    if abs(altotint/bbh_ltot-1) > 1e-
8:
                        print('bbh angular momentum problem',altotint,bbh_ltot)
                        raise SystemExit


                    for i in range(2):
                    #     Rotations as described here
https://youtu.be/N_njPJYaXaU?t=1983
                    #     First rotate around z-axis by the argument of periapsis
                        if i==0:
                            xold=bbh_deltax1
                            yold=bbh_deltay1
                            vxold=bbh_deltavx1
                            vyold=bbh_deltavy1
                        else:
                            xold=bbh_deltax2
                            yold=bbh_deltay2
                            vxold=bbh_deltavx2
                            vyold=bbh_deltavy2
                        zold=0
                        vzold=0
                        xnew=np.cos(bbh_argperi)*xold-np.sin(bbh_argperi)*yold
                        ynew=np.sin(bbh_argperi)*xold+np.cos(bbh_argperi)*yold
                        znew=zold
                        vxnew=np.cos(bbh_argperi)*vxold-np.sin(bbh_argperi)*vyold
                        vynew=np.sin(bbh_argperi)*vxold+np.cos(bbh_argperi)*vyold
                        vznew=vzold
                    #     Next rotate around y-axis by the inclination angle
                        xold=xnew
                        yold=ynew
                        zold=znew
                        vxold=vxnew
                        vyold=vynew
                        vzold=vznew
                        xnew=np.cos(bbh_inclination)*xold-
np.sin(bbh_inclination)*zold
                        ynew=yold
                        znew=np.sin(bbh_inclination)*xold+np.cos(bbh_inclination)
*zold
                        vxnew=np.cos(bbh_inclination)*vxold-
np.sin(bbh_inclination)*vzold
```

```
                        vynew=vyold
                        vznew=np.sin(bbh_inclination)*vxold+np.cos(bbh_inclinatio
n)*vzold
                    #     Finally rotate around z-axis by the longitude of
ascending node
                        xold=xnew
                        yold=ynew
                        zold=znew
                        vxold=vxnew
                        vyold=vynew
                        vzold=vznew
                        xi=np.cos(bbh_longitude)*xold-np.sin(bbh_longitude)*yold
                        yi=np.sin(bbh_longitude)*xold+np.cos(bbh_longitude)*yold
                        zi=zold
                        vxi=np.cos(bbh_longitude)*vxold-
np.sin(bbh_longitude)*vyold
                        vyi=np.sin(bbh_longitude)*vxold+np.cos(bbh_longitude)*vyo
ld
                        vzi=vzold
                        if i==0:
                            r2_0 = np.array([xi, yi, zi])
                            v2_0 = np.array([vxi, vyi, vzi])
                        else:
                            r3_0 = np.array([xi, yi, zi])
                            v3_0 = np.array([vxi, vyi, vzi])
                    if verbosity > 0:
                        print('After rotation, compact object 1 starts with
(relative to binary c.o.m.):')
                        print('                  r2_0=',r2_0)
                        print('                  v2_0=',v2_0)
                        print('After rotation, compact object 2 starts with
(relative to binary c.o.m.):')
                        print('                  r3_0=',r3_0)
                        print('                  v3_0=',v3_0)


                    # DONE WITH BBH
                    # NOW THINK ABOUT THE INTRUDER STAR

                    initialConditionsSaved = False

                    # Set the initial conditions:
                    r1 = np.array([deltax1, deltay1, 0])
                    v1 = np.array([deltavx1, deltavy1, 0])
                    r2 = np.array([r2_0[0]+deltax2, r2_0[1]+deltay2, r2_0[2]])
```

```
                    v2 = np.array([v2_0[0]+deltavx2, v2_0[1]+deltavy2, v2_0[2]])
                    r3 = np.array([r3_0[0]+deltax2, r3_0[1]+deltay2, r3_0[2]])
                    v3 = np.array([v3_0[0]+deltavx2, v3_0[1]+deltavy2, v3_0[2]])

                    #     prepare leap-frog scheme for first iteration:

                    if verbosity > 0:
                        print("star:", r1, v1)
                        print("BH1:", r2, v2)
                        print("BH2:", r3, v3)

                    a1, a2, a3, dt, d12, d13, d23 =
gravitational_acceleration(r1, r2, r3)

                    ekin = 0.5*(am1*np.linalg.norm(v1)**2 + bbh_m1 *
np.linalg.norm(v2)**2 + bbh_m2*np.linalg.norm(v3)**2)
                    epot = -G*am1*bbh_m1/d12 -G*am1*bbh_m2/d13 -
G*bbh_m1*bbh_m2/d23
                    mom0 = am1*v1 + bbh_m1*v2 + bbh_m2*v3
                    etot0 = ekin + epot

                    if verbosity > 0:
                        print(a1, a2, a3, dt)
                        print(f"Initial total energy = {etot0}")

                    dth = 0.5 * dt # half of  timestep
                    t = 0

                    # Update veloities with a half-step
                    v1[:3] += dth * a1[:3] # star
                    v2[:3] += dth * a2[:3] # BH1
                    v3[:3] += dth * a3[:3] # BH2

                    while rT1 < d12 <= sep0+bbh_semimajoraxis and rT2 < d13 <=
sep0+bbh_semimajoraxis:
                        # Update position with a full-step
                        #r1[:3] += dt * (v1[:3] + 0.5 * a1[:3] * dt) # star
                        #r2[:3] += dt * (v2[:3] + 0.5 * a2[:3] * dt) # BH1
                        #r3[:3] += dt * (v3[:3] + 0.5 * a3[:3] * dt) # BH2
                        r1[:3] += dt * v1[:3] # star
                        r2[:3] += dt * v2[:3] # BH1
                        r3[:3] += dt * v3[:3] # BH2

                        # store "old" velocites
                        v1o = np.array([v1[0], v1[1], v1[2]])
```

```
                        v2o = np.array([v2[0], v2[1], v2[2]])
                        v3o = np.array([v3[0], v3[1], v3[2]])

                        # Update veloities with a half-step (for purposes of
calculating energy and momentum)
                        dth = 0.5 * dt
                        v1[:3] = v1o[:3] + dth * a1[:3] # star
                        v2[:3] = v2o[:3] + dth * a2[:3] # BH1
                        v3[:3] = v3o[:3] + dth * a3[:3] # BH2

                        t += dth

                        a1, a2, a3, dt, d12, d13, d23 =
gravitational_acceleration(r1, r2, r3)

                        ekin = 0.5*(am1*np.linalg.norm(v1)**2 + bbh_m1 *
np.linalg.norm(v2)**2 + bbh_m2*np.linalg.norm(v3)**2)
                        epot = -G*am1*bbh_m1/d12 -G*am1*bbh_m2/d13 -
G*bbh_m1*bbh_m2/d23
                        mom = am1*v1 + bbh_m1*v2 + bbh_m2*v3
                        etot = ekin + epot
                        if (d12 <= 10*rT1 or d13 <= 10*rT2) and not
initialConditionsSaved:
                            maybePrintThis = f"{am1}\n"
                            maybePrintThis += f"{r1[0]} {r1[1]} {r1[2]}\n"
                            maybePrintThis += f"{v1[0]} {v1[1]} {v1[2]}\n"
                            maybePrintThis += f"{bbh_m1}\n"
                            maybePrintThis += f"{r2[0]} {r2[1]} {r2[2]}\n"
                            maybePrintThis += f"{v2[0]} {v2[1]} {v2[2]}\n"
                            maybePrintThis += f"{bbh_m2}\n"
                            maybePrintThis += f"{r3[0]} {r3[1]} {r3[2]}\n"
                            maybePrintThis += f"{v3[0]} {v3[1]} {v3[2]}\n"
                            t_10rT = t
                            maybePrintThis += f"\n The above data are for t =
{t}, delta e_tot = {etot-etot0}, delta momentum = {mom-mom0}\n"
                            initialConditionsSaved = True
                            if abs(etot/etot0-1) > 1e-5:
                                maybePrintThis += f"WARNING: ENERGY CONSERVATION
MIGHT NOT BE GOOD ENOUGH\n"
                            #print(f"{t:<9.3f} {d12:<10.3f} {d13:<10.3f}
{d23:<10.3f} {etot:<10.3f} {radius1:<10.3f}")

                        # Update veloities with two half-steps
                        v1[:3] = v1o[:3] + (dth + 0.5*dt) * a1[:3] # star
                        v2[:3] = v2o[:3] + (dth + 0.5*dt) * a2[:3] # BH1
```

```
                        v3[:3] = v3o[:3] + (dth + 0.5*dt) * a3[:3] # BH2

                        t += 0.5*dt
                    if (d12 <= rT1 and icol2 == 2) or (d13 <= rT2 and icol2 ==
3):
                        file.write(maybePrintThis)
                        #print(f"Passed within tidal radius {rT1:<10.3f} or
{rT2:<10.3f}: {t:<9.3f} {bbh_inclination:<10.3f} {bbh_trueanomaly:<10.3f}
{bbh_argperi:<10.3f} {bbh_longitude:<10.3f} {d12:<10.3f} {d13:<10.3f}
{d23:<10.3f} {etot:<10.3f} {radius1:<10.3f}")
                        file.write(f"Passed within tidal radius rT1={rT1:<10.3f}
or rT2={rT2:<10.3f}: t={t:<9.3f} i={bbh_inclination_degrees:<10.3f}
trueanomaly={bbh_trueanomaly_degrees:<10.3f} argperi={bbh_argperi_degrees:<10.3f}
longitude={bbh_longitude_degrees:<10.3f} d12={d12:<10.3f} d13={d13:<10.3f}
d23={d23:<10.3f} etot={etot:<10.3f} radius1={radius1:<10.3f}\n")
                        if t-t_10rT > 100:
                            file.write(f"WARNING: COLLISION OCCURS AT A TIME
{round(t-t_10rT)} after the start of the SPH CALCULATION\n")
    sys.stdout = sys.__stdout__
```